Die approbierte Originalversion dieser Dissertation ist in der Hauptbibliothek der Technischen Universität Wien aufgestellt und zugänglich.
http://www.ub.tuwien.ac.at

The approved original version of this thesis is available at the main library of the Vienna University of Technology.
http://www.ub.tuwien.ac.at/eng

TECHNISCHE UNIVERSITÄT WIEN
Vienna University of Technology

DISSERTATION

AMMONIA AS ENERGY STORAGE CARRIER IN CSP POWER PLANT WITH POWER TOWER RECEIVER

Submitted by

Ramadan Ali Abdiwe

In partial fulfillment of the requirements for the degree of

Doctor of Technical Science

Supervised by

Prof. Markus Haider

Institute for Energy Systems and Thermodynamics
Vienna University of Technology
Vienna, Austria

December, 2017

Abstract

The actual thesis had the objective of analyzing Power Tower CSP plant with thermochemical storage. To investigate the generation efficiency in the power generation system an exergy analysis on each component of the Central Receiver System (CRS) was conducted. With the exergy analysis it was shown where we should be focusing our efforts to improve system efficiency. EBSILON®Professional software was used in this study to obtain the exergy efficiency and the irreversibility in each component of a hypothetic CRS power plant to pinpoint the causes and locations of the thermodynamic imperfection. The obtained results show that at a constant DNI the maximum exergy loss occurs at the Solar Tower Receiver (STR). The performance of the STR affects significantly the efficiency of the entire solar power generation system and minimizing the heat loss of the STR plays a dominant role in increasing its performance. The simulation tool ANSYS® FLUENT® was used to compare the heat loss in an external type receiver and a cavity type receiver. The result showed that the heat losses in the external receiver are much higher than the heat losses in the cavity receiver making the cavity receiver a better option for increasing the power generation efficiency of the CRS.

Other major challenge is the increase of the system efficiency of the energy storage method. Thermochemical concept seems to offer an attractive solution to this problem. A thermochemical conversion of solar energy into chemical fuels offers an efficient path for long term storage and long-range transport of solar energy. In this study a thermochemical system using ammonia as energy storage carrier is investigated. A transient mathematical model using MATLAB software was developed to predict the behavior of the ammonia closed-loop storage system including but not limited to the ammonia solar reactor and the ammonia synthesis reactor. The MATLAB model contains transient mass and energy balances as well as a chemical equilibrium model for each relevant system component. For the importance of the dissociation and formation processes in the system, a Computational Fluid Dynamics (CFD) simulation on the ammonia solar and synthesis reactors has been performed. The CFD commercial package FLUENT is used for the simulation study and all the important mechanisms for packed bed reactors are taken into account, such as momentum, heat and mass transfer, and chemical reactions. The FLUENT simulation reveals the profiles inside both reactors and compared them with the profiles from the MATLAB model. The good agreement between both models gives hope for the feasibility of the design.

List of publications

This thesis is based on the work contained in the following papers, referred to by Roman numerals in the text.

I. Abdiwe, R., Haider, M. 2017. “Design of an ammonia closed-loop storage system in a CSP power plant with a power tower cavity receiver”. AIP Conference Proceedings 1850, 090001 (2017); doi: 10.1063/1.4984450.

II. Abdiwe, R., Haider, M. 2016. “A mathematical model for ammonia solar and synthesis reactors”. Renewables: Wind, Water, and Solar, 3:12

III. Abdiwe, R., Haider, M. 2015. “Investigation on the exergy performance of a central receiver power plant”. J Fundamentals of Renewable Energy Appl, 5: 168.

IV. Abdiwe, R., Haider, M. 2015. “Investigations on Heat Loss in Solar Tower Receivers with Wind Speed Variation”. International Journal of Sustainable and Green Energy. Vol.4, No. 4, 2015, pp. 159-165.

Ramadan Abdiwe is the principle author and investigator in all papers. Prof. Markus Haider has supervised the work in all papers and contributed to their writing.

Acknowledgements

After an intensive period of four years, today is the day: writing this note of thanks is the finishing touch on my thesis. It has been a period of intense learning for me, not only in the scientific area, but also on a personal level. Writing this thesis has had a big impact on me. I would like to reflect on the people who have supported and helped me so much throughout my PhD study.

I would first like to acknowledge the financial support given by the Libyan embassy in Austria during the entire period of my study at Vienna University of Technology (TU). I also would like to thank my colleagues from the institute for energy systems and thermodynamics at TU for their wonderful collaboration. I would particularly like to single out my supervisor professor Markus Haider for his excellent cooperation and for all the opportunities I was given to conduct my research and further my thesis at the institute for energy systems and thermodynamics. He definitely provided me with the tools that I needed to choose the right direction and successfully complete my thesis. Additional recognition is given to Dr. Ibrahim Alghariani from the Libyan embassy, and Michael Laurmann from TU who supported me greatly and were always willing to help me during my study. My research would not have been possible without their help.

I would also like to thank my family in Libya; my parents, sisters, and brothers. They were always supporting me and encouraging me with their best wishes.

Finally, I would like to thank my wife; Olga Palaznik. She was always there cheering me up and stood by me.

Thank you very much, everyone!

Table of contents

Chapter 1 – Introduction

1.1 Scope: Ammonia closed-loop storage system

Thermochemical conversion of solar energy into chemical fuels offers an efficient path for long term storage and long-range transport of solar energy [1]. With decades of research the ammonia dissociation and synthesis system is one of the more advanced concept thermochemical energy systems. The basic principle of the ammonia closed-loop storage system is based on the reversible dissociation of ammonia. Instead of storing heat by increasing the temperature of a substance or changing its physical state as the case of other CSP existing storage methods, an ammonia closed-loop storage system uses a reversible reaction to store energy in chemical bonds. The concept of using ammonia thermochemical storage system in concentrating solar power systems was first proposed at the Australian National University (ANU). The solar thermal group at (ANU) has been working for over three decades on a system for dissociating ammonia with concentrated solar energy so that the products can be stored and recycled through a conventional ammonia synthesis converter to achieve continues generation of electricity [2]. The industrial maturity of the ammonia synthesis tended to make researchers focus more on the ammonia dissociation part. Recently C. Chen, K. Lovegrove, and A. Lavine at the University of California have proposed a preliminary design of an ammonia synthesis system that is intended to heat steam from (350 ℃) to (650 ℃) making it suitable for a supercritical steam Rankine cycle power block [3]. Figure (1) shows a Schematic of ammonia dissociation, storage, and synthesis system. In this design the ammonia is used as a heat transfer fluid at the solar receiver side and as a product at the synthesis reactor side. The heat recovery process at the synthesis associated with the formation of ammonia can be used to produce steam required for electricity generation.

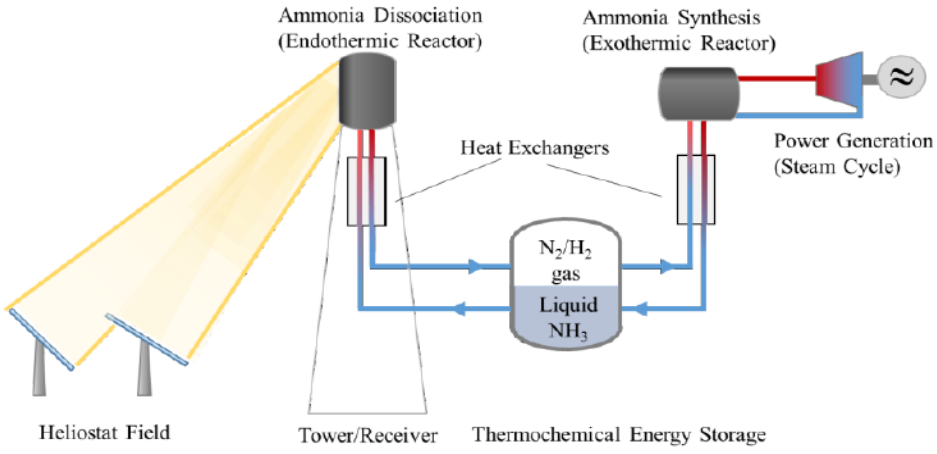

FIGURE 1. Schematic of ammonia dissociation, storage, and synthesis system [3]

As shown in the figure above, the reactants pass through endothermic and exothermic reactors; where the dissociation and the formation of the ammonia take place respectively. In between the reactors there is a storage container (vessel). The vessel is attached to counter-flow heat exchangers between ingoing and outgoing reactors. The ammonia is dissociated at the solar reactor and formed at the synthesis reactor according to the reversible reaction.

$$NH_3 + \Delta H \leftrightarrow 0.5N_2 + 1.5H_2 \qquad [\Delta H = 66.8\ kJ/mol] \tag{1}$$

Even though ammonia had been studied as energy carrier in CSP technologies in the last three decades, few papers were published on this topic. In 1995 Luzzi concluded that dish-based solar thermal systems, which incorporate the ammonia-based closed-loop thermochemical energy storage and transport technology, are technically viable using commercially available system components [2]. In 1998 Kreetz did an exergy analysis of a ($30\ MPa$) isobaric system. His exergy analysis revealed that the major irreversibilities occur within the exothermic reactor and the counter flow heat exchanger between ingoing and outgoing reactors [4]. In 2003 Lovegrove completed an experimental solar driven ammonia-based closed-loop thermochemical energy storage system and the system used a cavity receiver containing 20 reactor tubes filled with iron based catalyst material. Lovegrove concluded that ammonia dissociation receiver/reactors are well suited for operation through solar transients and that ammonia synthesis heat recovery reactors are capable of stable, predictable operation with heat recovery at temperatures suitable for high quality superheated steam production. However, using such system in large scale power plants might be challenging not only from the design point of view but also the parameters that ensure the maximum possible efficiency. Therefore, the optimal parameters such as mass flow rate and pressure of the whole system are of great interest. In 2016 Abdiwe [5] developed a mathematical model of ammonia solar and synthesis reactors and concluded that maintaining the best mass flow rate is important for achieving the maximum ammonia dissociation and formation processes and as a result the maximum thermal output. Furthermore operating the reactors at higher pressure than suggested increases the formation of ammonia at the synthesis, however it lowers the thermal output of the system.

In this study a mathematical model was developed for the ammonia closed-loop storage system including but not limited to the ammonia solar reactor and the ammonia synthesis reactor to predict the behavior of the reaction process inside both reactors. For the importance of the ammonia dissociation and formation processes in the system a Computational Fluid Dynamics (CFD) simulation on the ammonia solar and synthesis reactors has been performed to compare the result from the MATLAB model and the CFD model. It should be mentioned that the ammonia dissociation and formation processes contain several numbers of reactors; however, both models are designed for one tubular solar reactor and one tubular synthesis reactor.

Chapter 2 – Submodels

2.1 Physical Model

The performance of the Solar Tower Receiver (STR) affects significantly the efficiency of the entire solar power generation system and minimizing the heat loss of the STR plays a dominant role in increasing its performance. For the same absorbed area, the radiation loss in the cavity receiver is lower by almost (80%) than the radiation loss in the external receiver making the cavity receiver a more attractive option in STR technologies [6]. Therefore, the cavity receiver type was considered in this study. The geometry of the cavity receiver is assumed to have a cylindrical shape with a little base in the bottom to hold a bundle of solar reactors organized in a way that allows equal distribution of the solar flux between them. Figure (2) shows a schematic design of the cavity receiver with a bundle of solar reactors attached to it.

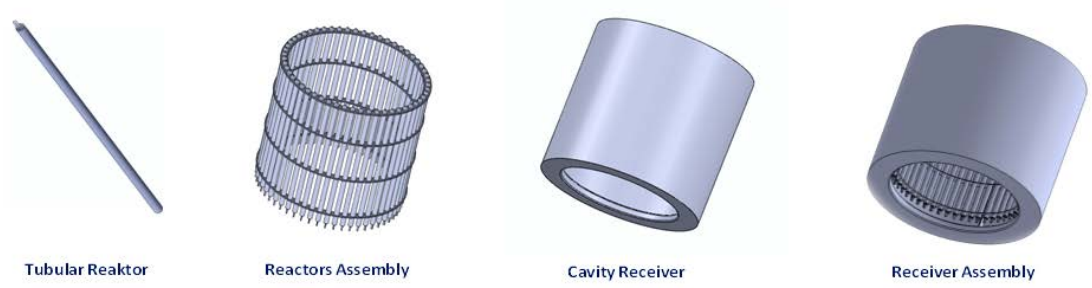

FIGURE (2). A schematic design of a solar cavity receiver

The solar and synthesis reactors as well as the heat exchangers and cooling pipes in both loops are assumed to be of tubular geometry type. Figure (3) shows longitudinal cuts of reactors, heat exchangers, and cooling pipes. The tubular reactors are filled up with catalysts to enhance the reaction rate.

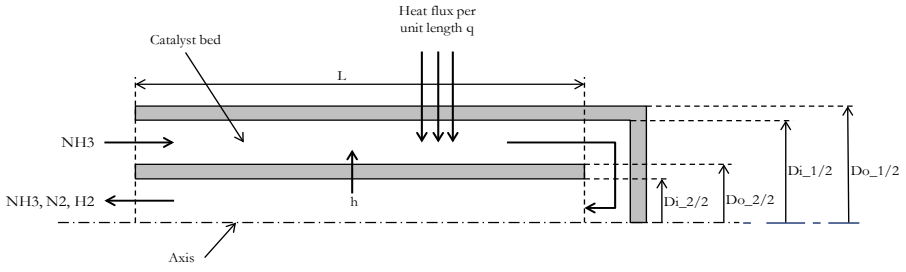

(a)

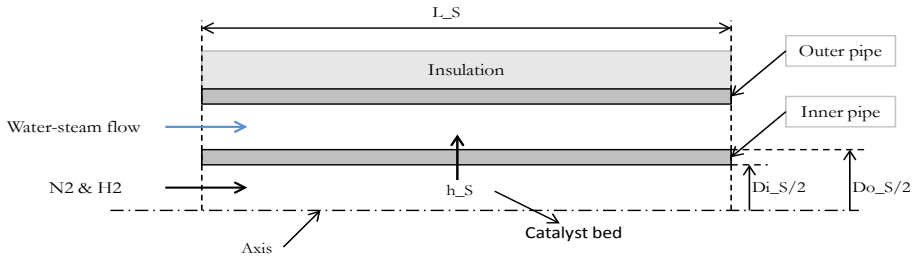

(b)

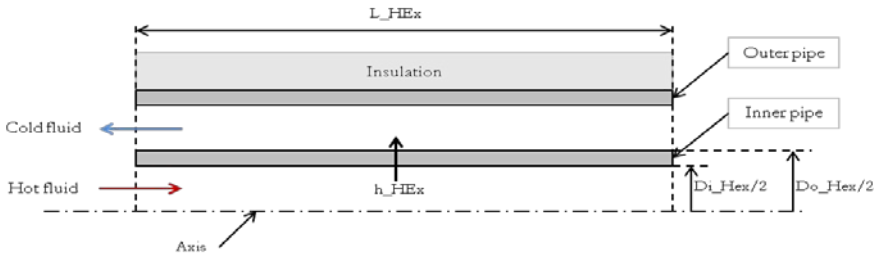

(c)

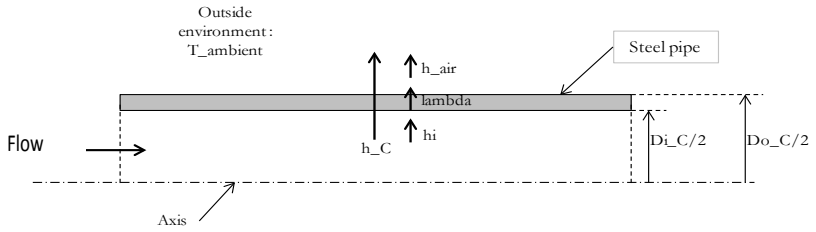

(d)

FIGURE 3. Geometries of the tubular: (a) solar reactor (b) synthesis reactor (c) heat exchanger (d) cooling pipe

Table (1) shows the physical parameters of the cavity receiver, ammonia solar reactor, ammonia synthesis reactor, catalyst bed, and vessel. The standard commercial catalyst material used a packed bed in both packed bed reactors is Iron-cobalt catalyst. Table (2) shows the properties of the catalyst.

TABLE 1. Geometry specifications of the main system components as analyzed

Item	Geometry Type	Dimensions
Cavity Receiver	Cylinder	Outer Diameter = 4.0 m Inner Diameter = 3.5 m Height = 4 m
Solar Tube dissociater Reactor	Tubular (tube in tube design)	Outer Diameter = 0.08166 m Inner Diameter = 0.06166 m Length = 3 m
Synthesis Tube Reactor	Tubular	Outer Diameter = 0.1 m Inner Diameter = 0.09 m Length = 3 m
Catalyst Bed (Iron-Cobalt)	Cylinder	Diameter = 0.0052 m Height = 0.0050 m
Vessel	Cylinder	Volume = 50 m^3

TABLE 2. The properties of the catalyst

Name	Iron-Cobalt
Chemical Composition	Al, % wt 25 Fe, % wt 24 Co, % wt 24 K, % wt 21
Impurities	S $< 200\ ppm$ CI $< 50\ ppm$
Physical Properties	Axial strength 400 kg/cm^2 Particle density 2.5 kg/l Filling density 1.6 kg/l
Activation Energy	$95E+03$ $[j/mol]$
Pre exponential Factor	$1E-2$ $[mol/s.cm^3.atm]$

Knowing the geometry of the cavity receiver the heat flux on solar reactor can be calculated as shown below:

$$Q_{rad,cavity} = \epsilon_{eff}.A_{ap}.E \tag{2}$$

$$E = \sigma.T^4 \tag{3}$$

$$T^4 = (T_{ab}^4 - T_{\infty}^4) \tag{4}$$

The effective emissivity (ϵ_{eff}) of the cavity receiver can be derived using the following equation [7]:

$$\epsilon_{eff} = \frac{1}{1+\left(\frac{1-\epsilon}{\epsilon}\right)\frac{A_{ap}}{A_{ab}}} \tag{5}$$

$$q = \frac{Q_{rad,cavity}}{A_{ab}} \quad (6)$$

In the synthesis side, the reaction is exothermic and the heat recovery process necessary to produce steam to generate electricity can be calculated thanks to the mature industry in producing ammonia.

2.2 Mathematical Model

The ammonia is dissociated endothermically to hydrogen and nitrogen by absorbing the solar energy at the cavity receiver during the daytime according to equation (1); the hot reactants will pass through the reactor's catalyst bed towards the vessel after exchanging their thermal energy in a counter-flow heat exchanger with the incoming ammonia. The temperature inside the vessel is above the ambient temperature saturation pressure of ammonia, therefore the ammonia will be condensed in the bottom of the vessel and the nitrogen and hydrogen stay at the top. During discharge, nitrogen and hydrogen mixture leave the vessel and react exothermically at standard ammonia synthesis to produce ammonia providing thermal energy for superheated steam production. In order for the reaction to occur during the dissociation and the formation stages, packed bed reactors are used with standard commercial catalyst material. Figure (4) shows the global system of the ammonia closed-loop storage. The system is divided into two loops, the solar reactor loop and the synthesis reactor loop. Figure (5) illustrates the main functions of the solar and synthesis reactor loops.

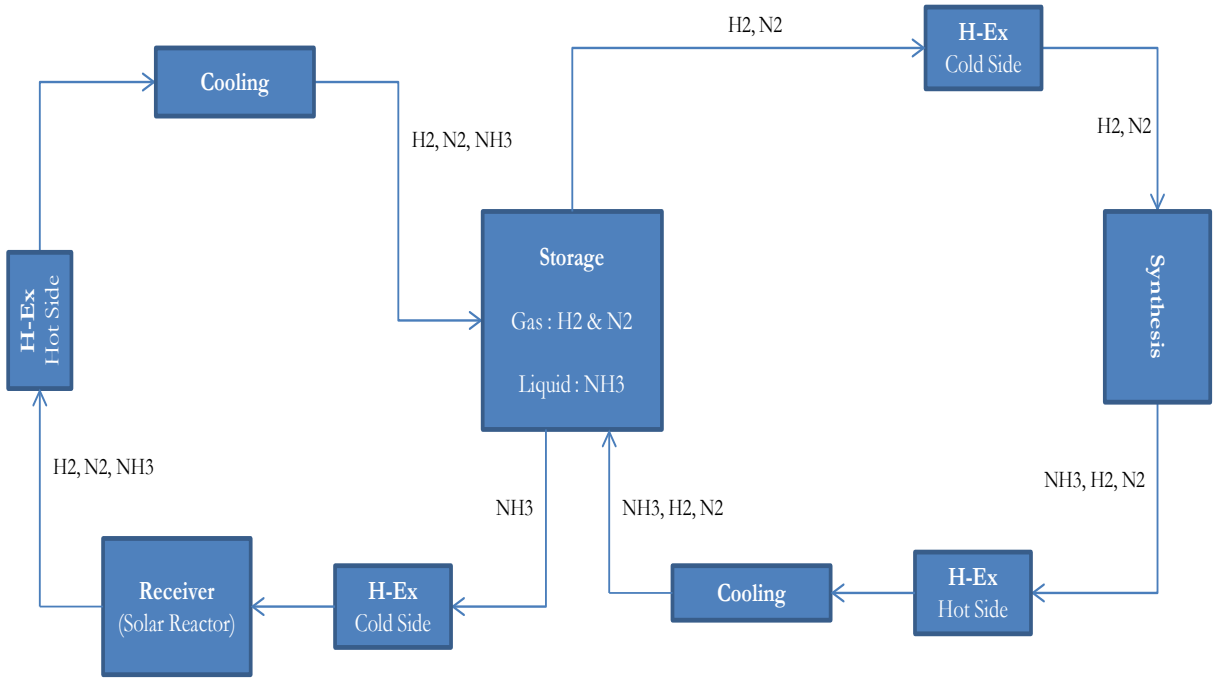

FIGURE 4. Global system of the ammonia closed-loop storage

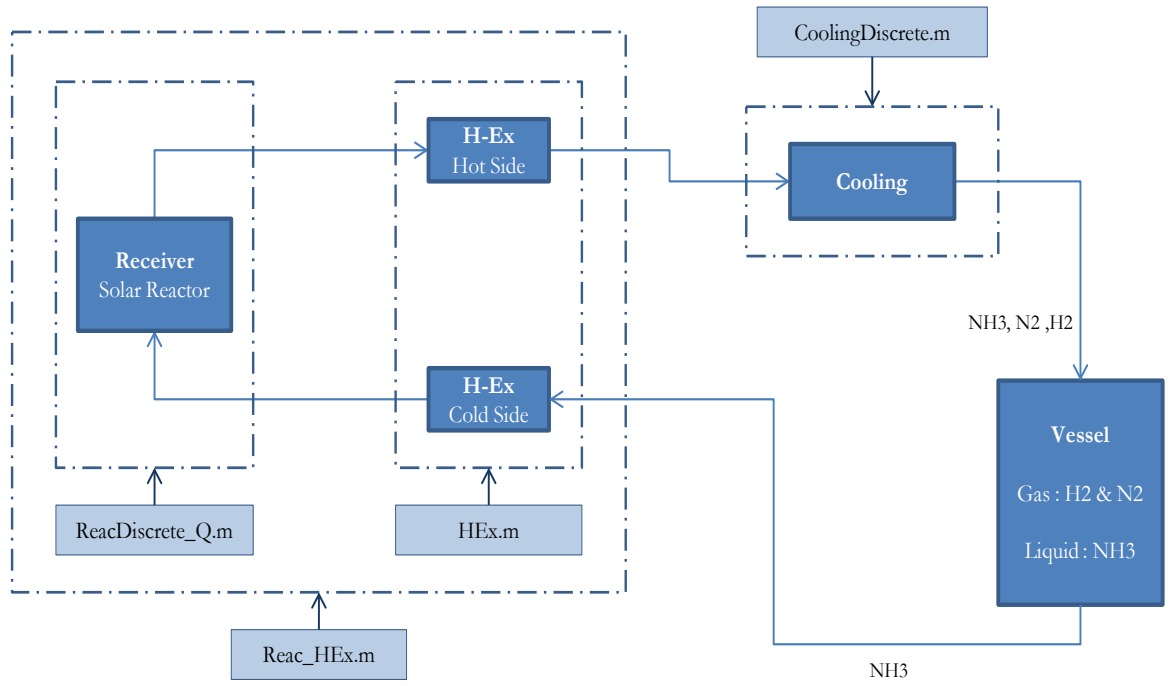

(a)

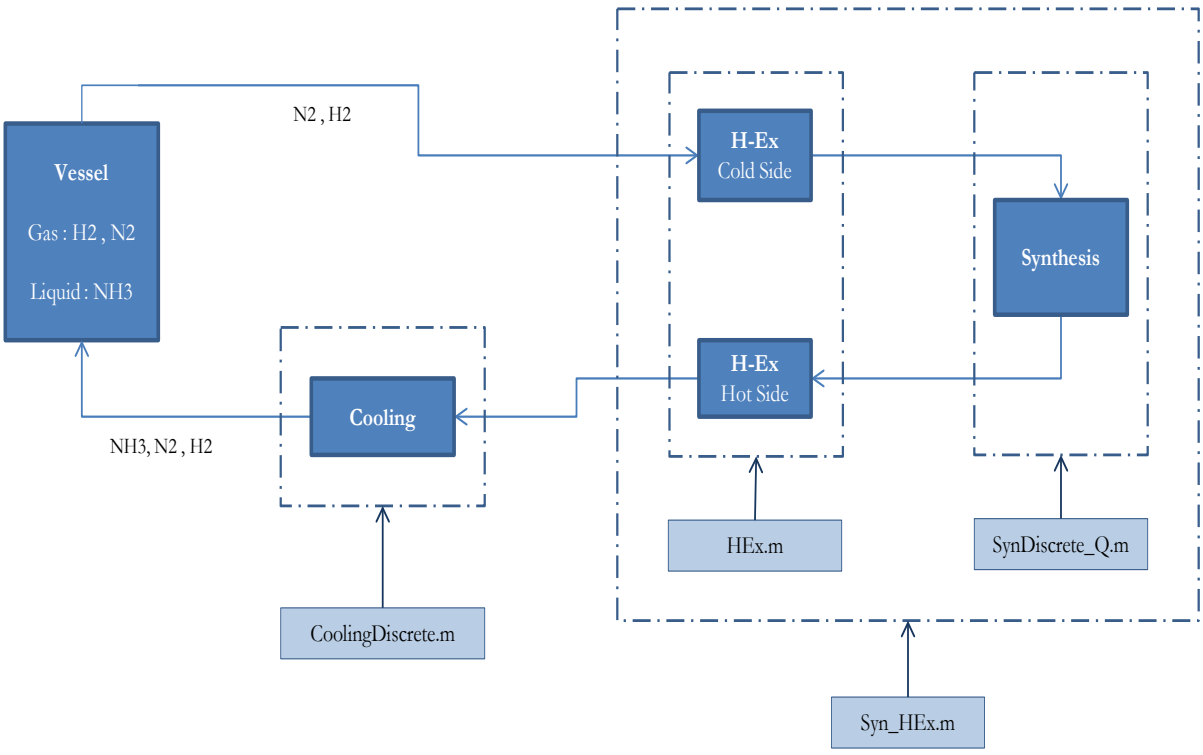

(b)

FIGURE 5. Main functions of (a) solar loop (b) synthesis loop

Figure (6) shows a simplified model of the ammonia closed-loop storage system including the reactors, heat exchangers, cooling pipes and vessel.

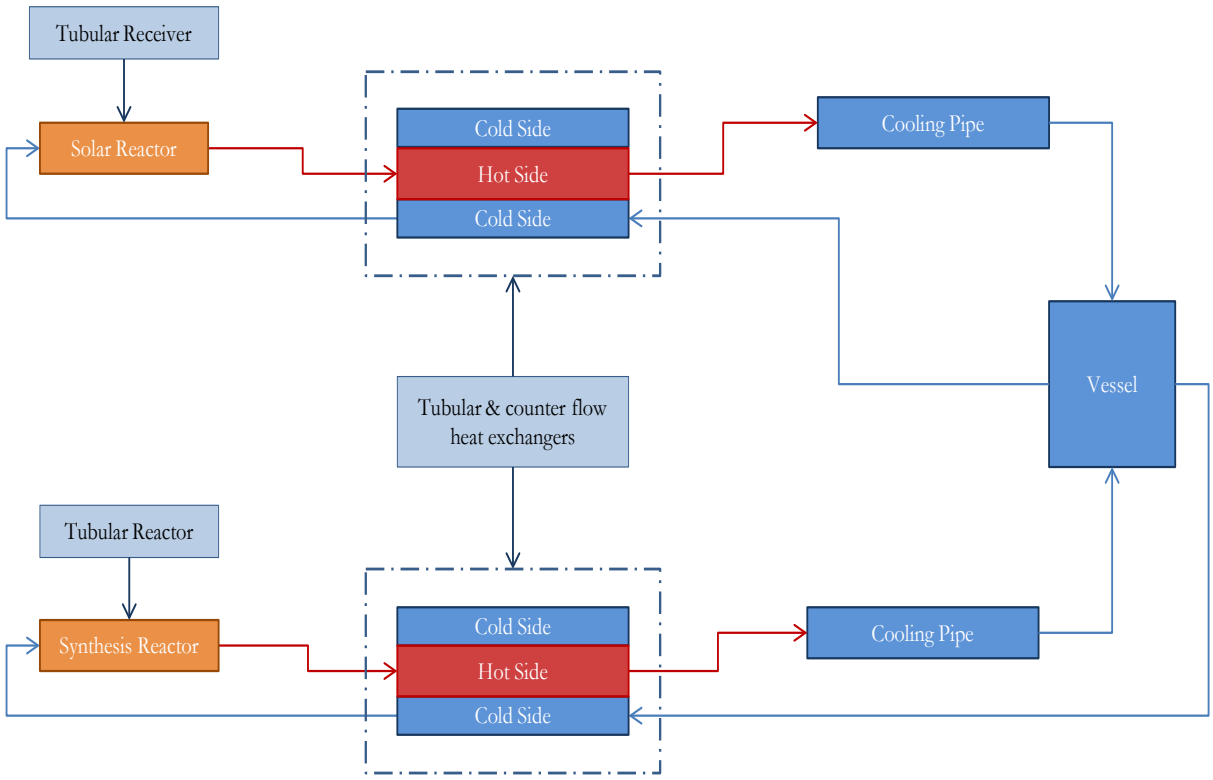

FIGURE 6. Simplified model of the ammonia closed-loop storage system

For any simple combustion where the number of possible species in the one exhaust stream matches the number of elements involved, the mass and energy balances allow predictive simulation behavior. However, in a general chemical reactor, additional information is required to predict the behavior of the reaction process and this information can be provided by functional equations. Typical examples for such equations are: pressure drop prescription, definitions of separation efficiencies, conversion rates, etc. These equations express the second law of thermodynamics taking in consideration that heat will always flow from the hot to the cold side and that chemical reactions always proceed towards an equilibrium state (with respect to temperature, pressure, and composition).

Several steps must be taken to implement equilibrium models such as the solar and synthesis reactors. Due to the similarity in both reactors, only the steps for the solar reactor will be explained as following:

1. Defining a control volume on the reactor

The control volume of the solar reactor is simple with one feed stream and one drain stream as shown in (Fig. 7). Both gas streams are modeled as ideal gases. The feed stream ideally consists of ammonia only, and the overall reaction scheme can be described by equation (1).

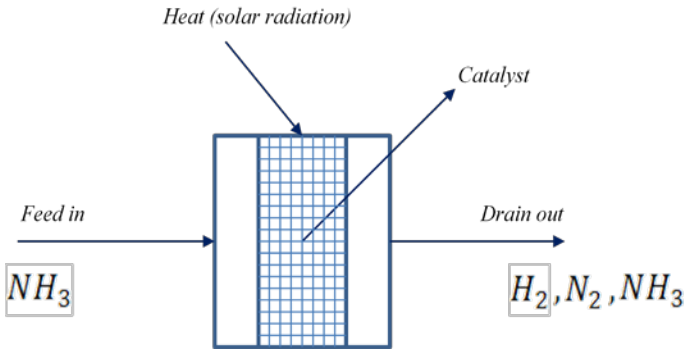

FIGURE 7. Sketch of solar reactor control volume.

Ammonia dissociation is limited by chemical equilibrium conditions in the drain. The syngas product contains three species: nitrogen N2, hydrogen H2, and ammonia NH3.

2. Summary of output variables attributed to determining equations

The output variables that are necessary for determining equations of the solar reactor are illustrated in table (3).

TABLE 3. Output variables

Symbol	Description	Determining equation
P_{drain}	Pressure drain stream	Pressure drop set
T_{drain}	Temperature at drain stream	Energy balance
n_{drain}	Total molar flow of drain stream	Global mass balance
$Y_{NH_3,drain}$	Drain stream ammonia content	Ammonia balance
$Y_{N_2,drain}$	Drain stream nitrogen content	Nitrogen balance
$Y_{H_2,drain}$	Drain stream hydrogen	Hydrogen balance

3. Modeling equations

The modeling equations can be illustrated as shown below:

a) Pressure drop [bar]

$$P_{drain} = P_{feed} - \Delta_p \tag{7}$$

b) Energy balance [W]

$$n_{drain} \,.\, H^*_{drain} = \, n_{feed} \,.\, H^*_{feed} + Q_{add} \tag{8}$$

H^* - represents the conventional enthalpy

Where

$$\mathrm{H^*_{drain}} = \sum_{\mathrm{i}} \mathrm{y_i} \,.\, \mathrm{H^*_i}\,(\mathrm{T_{drain}}) \tag{9}$$

c) Sum of drain mole fractions = 1 [mol/mol]

$$Y_{NH_3,drain} + Y_{H_2,drain} + Y_{N_2,drain} = 1 \tag{10}$$

d) Hydrogen balance $[\mathrm{mol_{H2}/s}]$

$$n_{drain} \cdot \left(Y_{H_2,drain} + \frac{3}{2}\, Y_{NH_3,drain}\right) = n_{feed} \cdot \frac{3}{2}\, Y_{NH_3,feed} \tag{11}$$

e) Nitrogen balance $[\mathrm{mol_{N2}/s}]$

$$n_{drain} \cdot \left(Y_{N_2,drain} + \frac{1}{2}\, Y_{NH_3,drain}\right) = n_{feed} \cdot \frac{1}{2}\, Y_{NH_3,feed} \tag{12}$$

f) Ammonia dissociation equilibrium [-]

$$K_{P,NH_3}(T_{drain}) = \frac{Y_{N_2,drain} \cdot Y^3_{H_2,drain}}{Y^2_{NH_3,drain}} \left(\frac{P_{drain}}{P_o}\right)^2 \tag{13}$$

K_P Is a function of temperature only and can be calculated from Gibbs free enthalpy of reaction according to:

$$ln\big(K_P(T)\big) = -\frac{\Delta G^o_R(T)}{R.T} \tag{14}$$

ΔG^o_R Is the Gibbs free enthalpy of standard pressure ($1\,bar$) and can be calculated from the conventional enthalpies and entropies of the participating species:

$$\Delta G^o_R = \sum_i [\nu_i . H^*_i(P_o.T)] - T. \sum_i [\nu_i . S_i(P_o.T)] \tag{15}$$

Therefore, equilibrium can be calculated directly from thermodynamic data.

4. Calculating strategy

In principle, the six output variables listed in step 2 together with equations in step 3 represent a fully determined system of algebraic, non linear equations. To solve such a system, a numerical method must be applied (MATLAB). When solving the model a good starting guess is required to obtain a solution and care must be taken to prevent any $Y_{i,drain}$ to get below zero at any time.

The same steps must be applied for the synthesis reactor taken into consideration that the reactants in the solar reactor are the products in the synthesis reactor and vice versa. The system operates under isochoric conditions, therefore a change in molar specific volume of the gas/ammonia mixture during operation of dissociation and formation reactions. No reaction occurs outside both reactors because the kinetic energy transferred is low making the molecules movement not fast enough to allow reactions. The values of the running parameters for a single tube reactor are shown in table (4).

TABLE 4. Simulation parameters

Parameter	Value
Mass Flow Rate	17 g/s
Pressure	50 bar
Inlet Gas Temperature in Both Reactors	250 $^{\circ}C$
Heat Flux Distributed in the Solar Reactor	100 kW

For the other components of the system where no reaction occurs such as the heat exchangers, cooling pipes, and vessel, an energy balance should be applied (this was done in a work project at Vienna technical university by Etienne Bertrand [8]). Figure (8) shows a sketch of a tubular counter flow heat exchanger control volume.

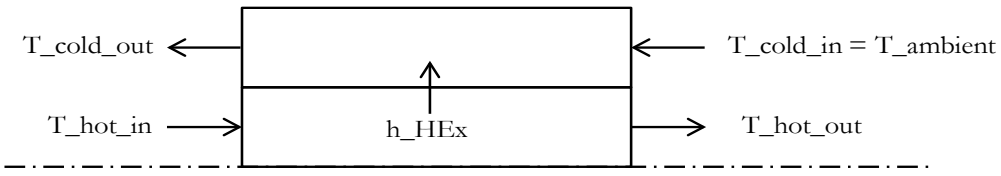

FIGURE 8. A sketch of a tubular counter flow heat exchanger control volume

Applying a global energy balance

$$q_{hot} * (T_{hot-in} - T_{hot-out}) = q_{cold} * (T_{cold-out} - T_{cold-in}) \quad (16)$$

$$q = \dot{m} * c_p \quad (17)$$

$T_{cold-in}$ - The temperature of the gas inside the vessel

$T_{cold-out}$ - The Inlet gas temperature in both reactors

T_{hot-in} - The temperature of the mixture leaves the reactor and calculated by reactor's function

$T_{hot-out}$ - The temperature of the ammonia enters the reactor calculated thanks to the global energy balance

$\dot{m}$ - The mass flow rate

c_p - The specific heat capacity

$$T_{hot-out} = T_{hot-in} - (q_{cold}/q_{hot}) * (T_{cold-out} - T_{cold-in}) \quad (18)$$

Surface area of the heat exchanger is then deduced from NTU method. Figure (9) shows the connection between the solar reactor and the heat exchanger.

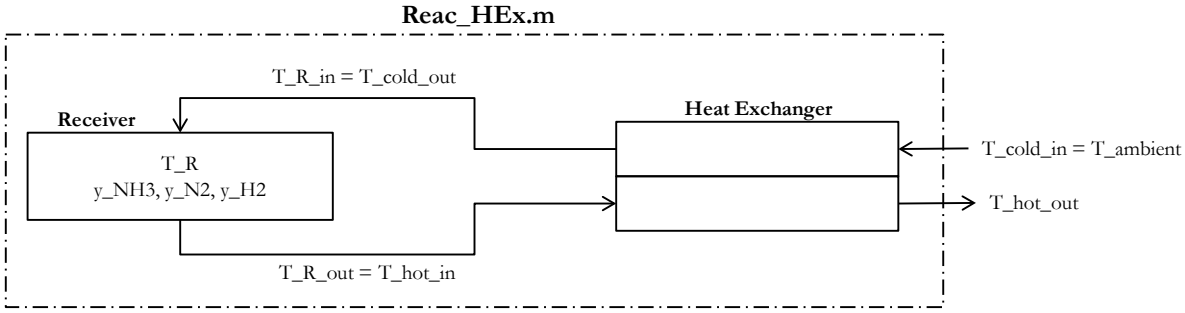

FIGURE 9. Connection between Receiver and Heat exchanger

When all geometric data specified and $T\_ambient$ and T_R_{in} are given, $Reac\_HEx.m$ function computes the temperature profile T_R, the three mol fraction profiles y_NH3, $\_N2$, y_H2, the outlet temperature $T_{hot-out}$ and the surface area of the heat exchanger.

$$[y\_NH3, y\_N2, y\_H2, T\_R, T_{hot-out}, S\_HEx] = Reac\_Hex\ (Molarflow, T\_ambient, T\_R\_in]$$

The following diagram resumes the connection between receiver and heat exchanger:

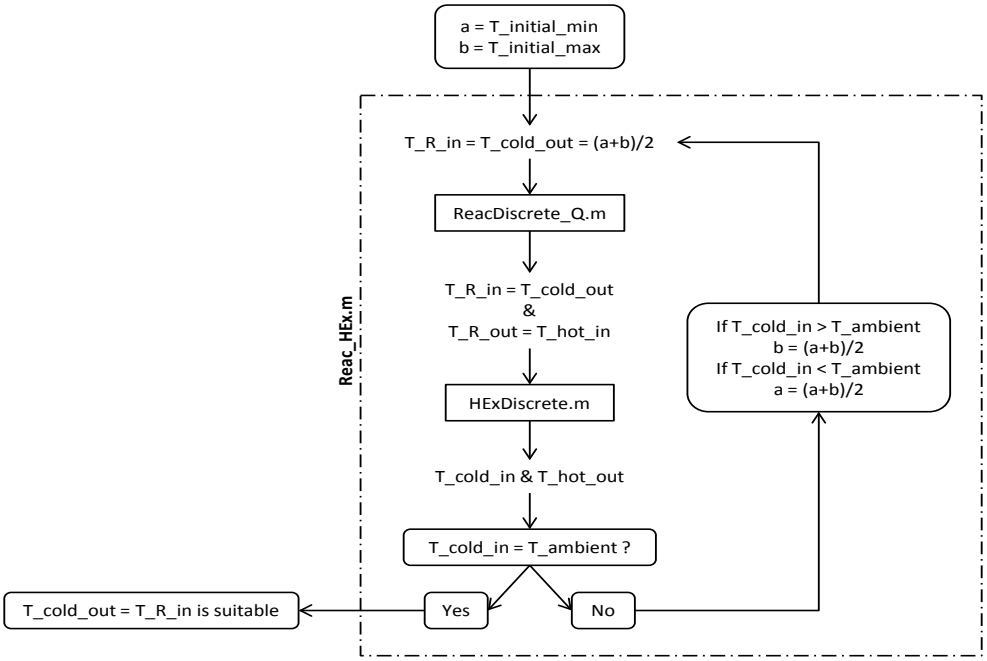

FIGURE 10. A diagram of the connection between the receiver and heat exchanger

Figure (11) shows a sketch of a tubular cooling pipe used between both receivers and the vessel.

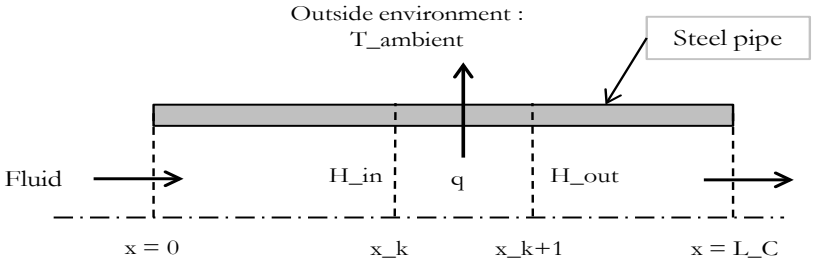

FIGURE 11. A sketch of a tubular cooling pipe

Heat exchanged per unit length is given by:

$$q = h_c * \pi * Do_c * (T_c - T_{ambient}) \tag{19}$$

h_c - The global heat transfer coefficient

Do_c - The outer diameter of the cooling pipe

T_c - The temperature of the cooling pipe

Applying an energy balance

$$H_{out} - H_{in} = -q * dx \tag{20}$$

Because of the similarity between solar and synthesis loops, the same can be done for the heat exchanger and the cooling pipe in the synthesis loop. In the vessel component which connects both loops, few assumptions were made:

a) Temperature is constant

b) Ammonia is mainly liquid

c) Nitrogen and Hydrogen are mainly gaseous

d) Nitrogen and Hydrogen are initially present in stoichiometric proportion

Based on the ammonia vapour diagram showing in the Figure (12) the ammonia around the blue zone is mainly liquid:

$$T_{vessel} = T_{ambient} = (20 - 30)\ ℃$$

$$P\_vessel\ = (15 - 60)\ bar$$

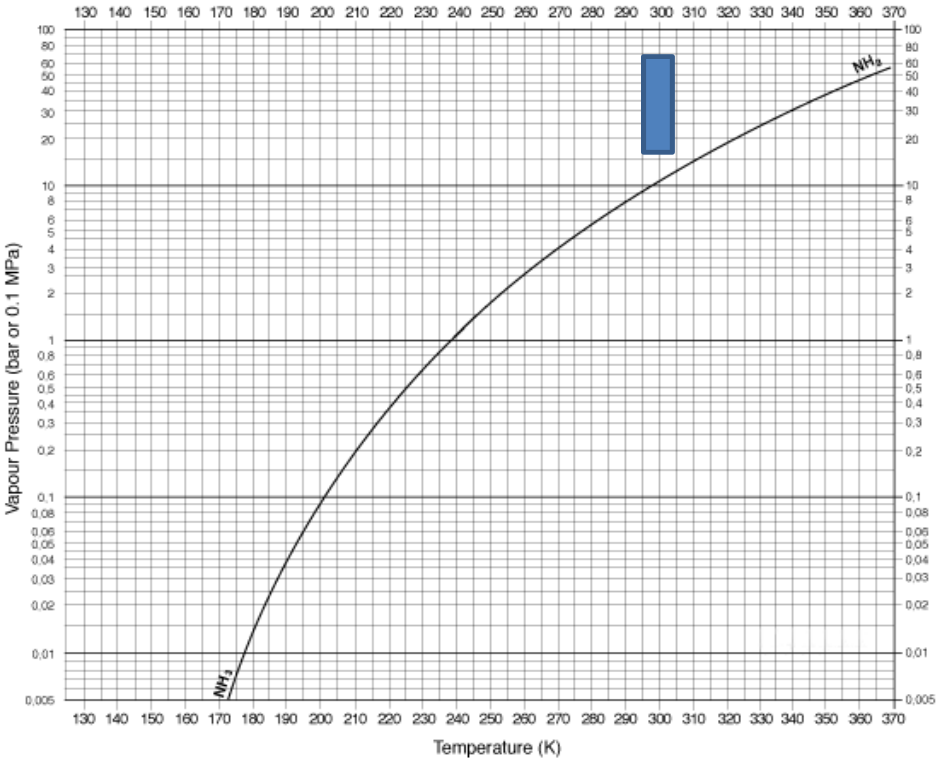

FIGURE 12. Ammonia vapour pressure diagram

As the case with the previous components, a control volume must be defined for the vessel to apply an energy balance. Figure (13) shows the inputs and outputs of the vessel

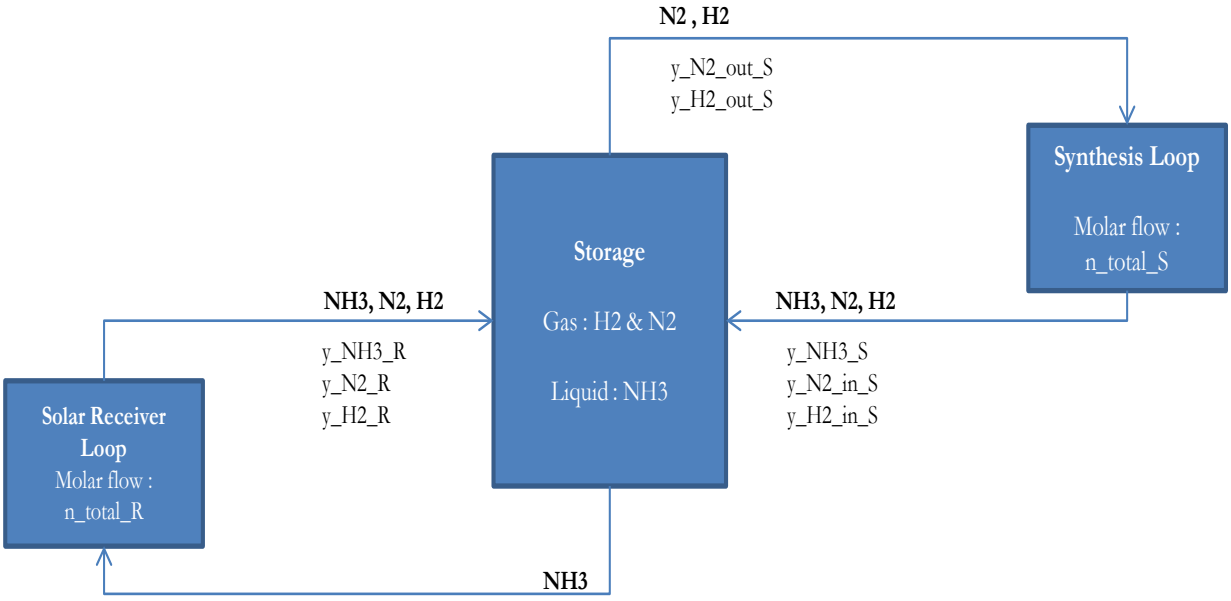

FIGURE 13. Inputs and outputs of the vessel

The liquid and vapour phases composition in the vessel must be illustrated. Nitrogen and hydrogen partial pressures can be calculated as following:

$$p_{N2} = (n_{N2} * R * T_{ambient})/V\_vap \quad (21)$$

$$p_{H2} = (n_{H2} * R * T_{ambient})/V\_vap \quad (22)$$

From Henry's law, the molar fractions of nitrogen and hydrogen in liquid phase can be calculated as following:

$$y\_L\_N2 = p\_N2/K\_N2 \quad (23)$$

$$y\_L\_H2 = p\_H2/K\_H2 \quad (24)$$

$$y\_L\_NH3 = 1 - (y\_L\_N2 + y\_L\_H2) \quad (25)$$

From Raoult's law, the molar fraction of ammonia in vapour phase can be calculated as following:

$$y\_V\_NH3 = y\_L\_NH3 * P\_sat\_NH3/p \quad (26)$$

When water is solvent, at $T\_ambient = 25°C$ the Henry's constants K_N2 and K_H2 and also for ammonia $NH3$ vapour pressure at 25 °$\boldsymbol{C}$ P_sat_NH3 ($\approx 9.5bar$) can be found [9].

Chapter 3 – Computational Fluid Dynamics Modeling

3.1 Governing Equations

For the importance of the dissociation and formation process in the system, a Computational Fluid Dynamics (CFD) simulation for both reactors has been performed to validate the MATLAB model. The commercial CFD software FLUENT solves the governing integral equations for conservation of mass, momentum, energy and other scalars such as turbulence and chemical species. The equation for conservation of mass, or continuity equation, can be written as follows [10]:

$$\frac{\partial \rho}{\partial t} + \nabla . (\rho \vec{v}) = S_m \tag{27}$$

Equation (27) is the general form of the mass conservation equation and is valid for incompressible as well as compressible flows. The source (S_m) is the mass added to the continuous phase from the dispersed second phase (e.g., due to vaporization of liquid droplets) and any user-defined sources. Conservation of momentum in an inertial (non-accelerating) reference frame is described by [10]:

$$\frac{\partial}{\partial t}(\rho \vec{v}) + \nabla . (\rho \vec{v} \vec{v}) = -\nabla p + \nabla . (\bar{\bar{\tau}}) + \rho \vec{g} + \vec{F} \tag{28}$$

Where p is the static pressure, $\bar{\bar{\tau}}$ is the stress tensor, and $\rho \vec{g}$ and $\vec{F}$ are the gravitational body force and external body forces respectively. $\vec{F}$ also contains other model-dependent source terms for porous-media.

In the employed CFD software package FLUENT [10], porous media are modeled by the addition of a source terms to the momentum equations of flow. The source term is composed of two parts: a viscous resistance loss and an inertial resistance loss. There are various forms of the momentum equation porous medium analogue to the Navier-Stokes equation. The commonly used Darcy's law is in refined and one dimensional form expressed as [11]:

$$\frac{dp}{dx} = -\frac{\mu}{K}\frac{Q}{A} \tag{29}$$

A is the area perpendicular to flow direction, K is the permeability, μ is the dynamic viscosity, and Q is the volume flow. The coefficient K, called permeability in single phase flow, is independent of the nature of the fluid and is exclusively given by geometry of the medium. Darcy's law is valid as long as Reynolds number based on average grain diameter does not exceed some value, often between 1 and 10 [12]. The fluid can be treated as incompressible and Newtonian and the porous medium is fixed.

When Reynolds number increases over a certain level, the pressure drop becomes higher than what is predicted by Darcy's equation. Non-linear terms are introduced in the so called Forchheimer equation which later had been modified by Ergun by fittings to experimental data according to [13].

$$\frac{\Delta p}{l} = 150\frac{(1-\varepsilon)^2}{\varepsilon^3}\frac{\mu U}{{D_p}^2} + 1.75\frac{(1-\varepsilon)}{\varepsilon^3}\frac{\rho U^2}{D_p} \tag{30}$$

The first term is the viscous loss D (proportional to velocity) and the second term is the inertial loss C (proportional to velocity squared). Compare this to the fluent expression for momentum sink:

$$\frac{\Delta p}{l} = D\mu U + \frac{1}{2}C\rho U^2 \tag{31}$$

$$D = \frac{150(1-\varepsilon)^2}{\varphi^2 {D_p}^2 \varepsilon^3} \tag{32}$$

$$C = \frac{3.5(1-\varepsilon)}{\varphi D_p \varepsilon^3} \tag{33}$$

φ is the sphericity of the cylindrical particles or pellets. The Ergun equation assumes that the bed is filled with uniform sized and shaped particles. The sphericity parameter is used as a conversion factor for non-spherical particles (comparing the surface volume ratio of these particles to an equivalent spherical particle) and for fully spherical particle, the sphericity equal one. In general the sphericity can be defined by:

$$\varphi = \frac{6}{D_p}\frac{S_p}{V_p} \tag{34}$$

For common shapes, like sand particles, sphericity can be around (0.8 – 0.9). From equation (30) a modified Reynolds ($Re^{"}$) number can be defined:

$$Re^{"} = \frac{\rho D_p U}{\mu}\frac{1}{(1-\varepsilon)} \tag{35}$$

Knowing the particle density and the filling density the porosity can be determined as following:

$$\varepsilon = 1 - \frac{\text{Filling density}}{\text{Particle density}} \tag{36}$$

The energy equation of gas phase and the energy equation of solid phase are coupled by a heat transfer coefficient:

$$h = \frac{Nu\lambda_g}{d_h} \tag{37}$$

In FLUENT a dual cell mesh technique is employed which allows a cell based heat transfer between the gas phase and the solid phase within the concept of porous medium treatment [14].
The general form of the conservation equation for chemical species in Fluent as following [10]:

$$\frac{\partial}{\partial t}(\rho Y_i) + \nabla.(\rho\vec{v}Y_i) = -\nabla.\vec{J_i} + R_i + S_i \tag{38}$$

Where R_i is the net rate of production of species i by chemical reaction and S_i is the rate of creation by addition from the dispersed phase plus any user-defined sources. $\vec{J_i}$ is the diffusion flux of species i, which arises due to gradients of concentration and temperature. The net source of chemical species i due to reaction R_i is computed as the sum of the reaction sources over the N_R reactions that the species participate in [15]:

$$R_i = M_{w,i}\sum_{r=1}^{N_R}\hat{R}_{i,r} \tag{39}$$

$M_{w,i}$ - The molecular weight of species i

$\hat{R}_{i,r}$ - The molar rate of creation/destruction of species i in reaction r

The reaction may occur as a volumetric reaction, a surface reaction, or a particles reaction. The r^{th} reaction can be written as:

$$\sum_{i=1}^{N} v'_{i,r}M_i \rightleftharpoons \sum_{i=1}^{N} v''_{i,r}M_i \tag{40}$$

M_i - The symbol denoting species i

N - The number of chemical species in the system

$v'_{i,r}$ - The stoichiometric coefficient for reactant i in reaction r

$v''_{i,r}$ - The stoichiometric coefficient for product i in reaction r

For our ammonia reaction

$$2NH_3 + dH \leftrightarrow N_2 + 3H_2 \tag{41}$$

$$M_1 = NH_3 \quad M_2 = N_2 \quad M_3 = H_2$$

$$v'_{1,r} = 2 \quad v'_{2,r} = 0 \quad v'_{3,r} = 0$$

$$v''_{1,r} = 0 \quad v''_{2,r} = 1 \quad v''_{3,r} = 3$$

The forward rate constant for reactionr, $k_{f,r}$ is computed using an expanded version of the Arrhenius expression:

$$k_{f,r} = A_r T^{\beta_r} e^{-\frac{E_r}{RT}} \quad (42)$$

The backward rate constant for reaction r, $k_{b,r}$ can be computed from the forward rate constant $k_{f,r}$ and the equilibrium constant for reaction K_r by the following equation:

$$k_{b,r} = k_{f,r}/K_r \quad (43)$$

The equilibrium constant for reaction can be extracted from the thermodynamic properties of the materials.

3.2 Geometric Model and Grid

A CFD model was developed to simulate the dissociation and formation of ammonia in regular fixed bed reactors. SolidWorks modeling package was used to draw the reactors (solar tubular reactor and synthesis reactor) separately then imported to the commercial CFD software FLUENT for meshing and simulating. The objective of designing the fixed bed reactor is to identify a set of system parameters for optimal operation. These parameters are temperature, pressure, composition, flow rate, dimensions of the reactor tube, and catalyst pellet.

The tubular packed bed reactor simulated has a tube in tube design. Figure (3 - a) shows a sketch of the solar reactor and the domain contains three regions. Entrance and exit are the extrusions to allow the flow to develop. The space between the outer tube and inner tube is filled with randomly arranged cylindrical catalyst where the reaction takes place. The reaction products leave through the inner tube in the middle and exchange the heat with the inner tube side of the catalyst.

The geometrical modeling is a critical stage in CFD simulation and in order to get more practical state for the simulation, the correct definition of the geometry must be provided. Also the technique used for constructing the geometry will ensure the feasibility of generating a mesh good enough to capture all of the phenomena involved in the problem. Tetrahedral grid is adopted for meshing the reactor and the total number of cells used for the reactor is about 2 millions cells. The model treated the catalyst as porous media fluid with user provided porosity, viscous resistance, inertial resistance, and effective diffusivity. The tubular outside wall is exposed to a constant heat flux which is provided from the heliostats to the cavity receiver that holds the ammonia tube reactors as shown in figure (5).

3.3 **Boundary Conditions**

The boundary conditions determine the flow and thermal variables on the boundaries of the physical model. The inlet (entrance) is modeled as velocity inlet and the outlet (exit) is modeled as pressure outlet. The reactor bed walls are maintained at a constant heat flux of ($100\,\mathrm{kW/m^2}$) and the domain operating pressure is assumed to be ($50\,bar$). The porous resistance coefficients are calculated using Ergun equation and the pressure drop is (0.48 bars). From equation (36) the porosity is found to be (0.36). The concentrations of the mixture species are given in the table (5). The inlet flow assumed as uniform and the inlet velocity and temperature are ($5\,m/s$) and (250 ℃) respectively. The flow is laminar in the porous media and turbulent in the remaining part of the domain. The turbulence is modeled by the standard $\mathrm{k}-\varepsilon$ turbulence model.

TABLE 5. Inlet concentrations of the species

Species	Mole Fraction
NH_3	100 [%]
N_2	0 [%]
H_2	0 [%]

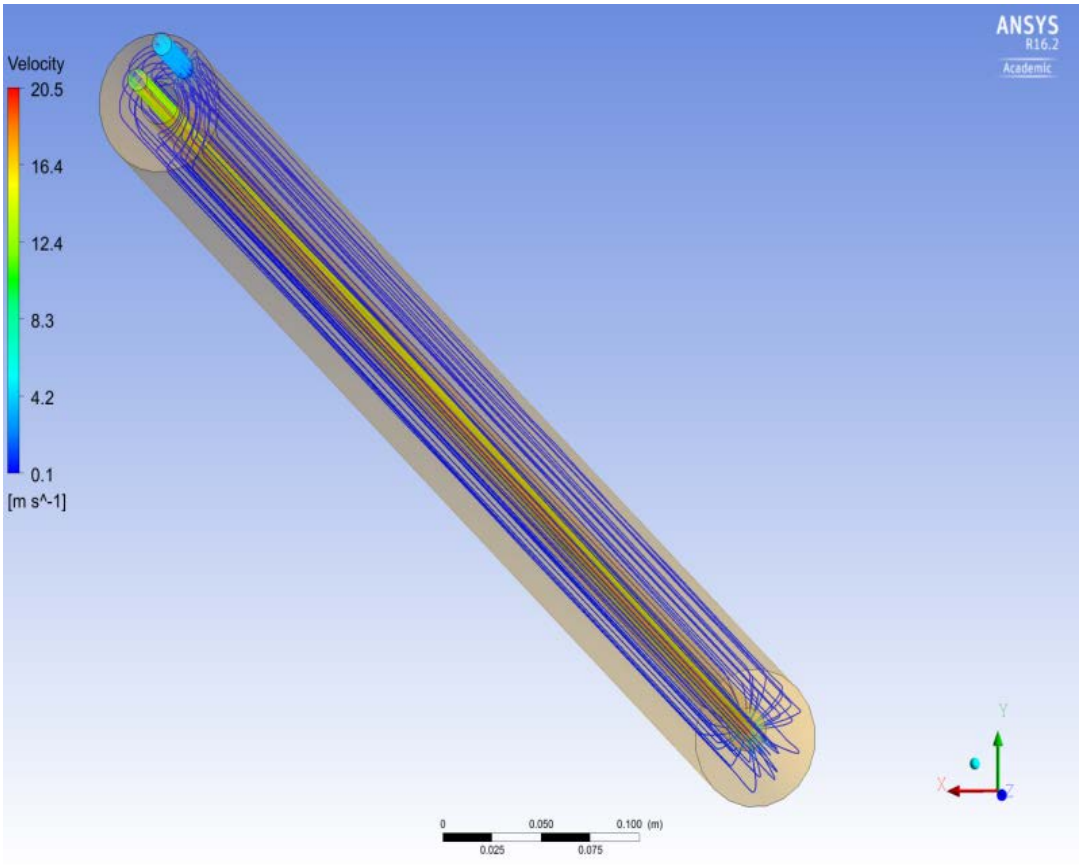

FIGURE 14. Velocity contour along the length of the solar tube reactor

Chapter 4 – Results

The dynamic behavior of the ammonia closed-loop storage system under a steady-state operation has been predicted with a MATLAB numerical model. Two important inputs for the model are the steam mass flow in the heat recovery process at the synthesis reactor, and the heat flux distributed on the solar reactor inside the cavity which has been derived based on the geometry of the cavity receiver. In the discharging case, the steam mass flow is the only inputs since no heat flux occurs at the solar receiver during night time. The model confirmed the technical feasibility of the design concept of the whole system. Figure (15) and (16) show modeled internal reactor temperature and corresponding reaction extent profiles of the reactants and products in both reactors. The horizontal axis shows the position along the catalyst bed as measured from the point of gas inlet.

The tube in tube design of the solar tube reactor allows the heat exchange between the gas mixture at exit and at inlet of the reactor as shown below in the temperature profile. The reaction in the solar receiver is endothermic and the temperature required for efficient dissociation depends on the catalyst. There is a wide variety of materials that has been found to be effective but some materials require high temperatures. The solar cavity receiver can provide the high temperatures needed for the ammonia dissociation (cracking) and also to overcome thermal losses in the reactor. An extreme increase in the solar reactor temperature is undesirable because it damages the reactor materials (catalyst and container); therefore, it is important to keep a small portion of ammonia not dissociated to prevent the overheating and keep the reactor bed at an optimum temperature.

The reaction in the synthesis reactor is typically carried out over catalysts at temperatures around 400-600 ℃ and pressures ranging from 200 to 400 bars. However, operating the ammonia closed-loop storage system at higher pressure than suggested for maximum ammonia production at the synthesis lowers the thermal output [5]. It’s important to emphasize that the thermal output from the synthesis in the ammonia closed-loop storage system is more important than producing maximum amount of ammonia. Therefore, our system operates at lower pressure to maintain the maximum thermal output.

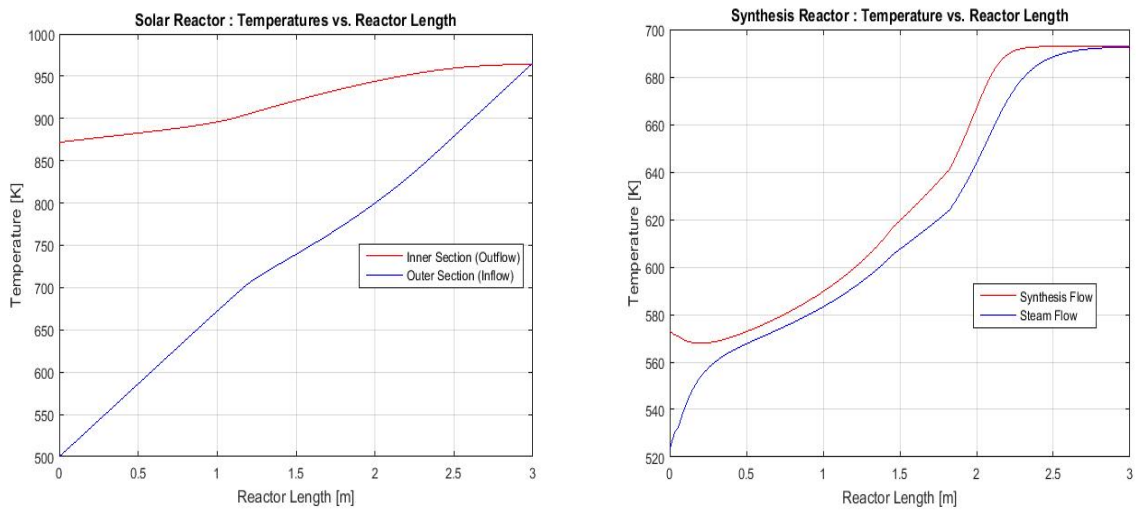

FIGURE 15. Temperature profiles in the solar and synthesis tube reactors (MATLAB model)

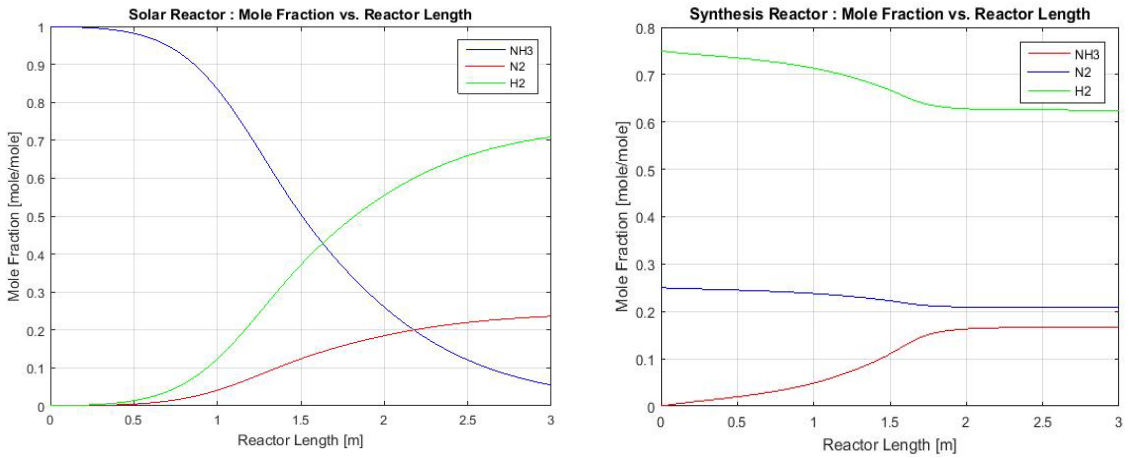

FIGURE 16. Mole fractions of the species along the solar and synthesis tube reactors (MATLAB model)

The CFD simulation results of the solar reactor indicate that the ammonia concentration has decreased due to the reaction occurring along the length of the reactor and the concentrations of the product species (Hydrogen and Nitrogen) have increased. Figures (17), (18), and (19) show the contours of the temperature, mass fraction of species, and the pressure at a longitudinal cut of the solar reactor, respectively. The higher pressure is located around the catalyst entrance and then the pressure drops through the catalyst due to the viscous and inertial resistance.

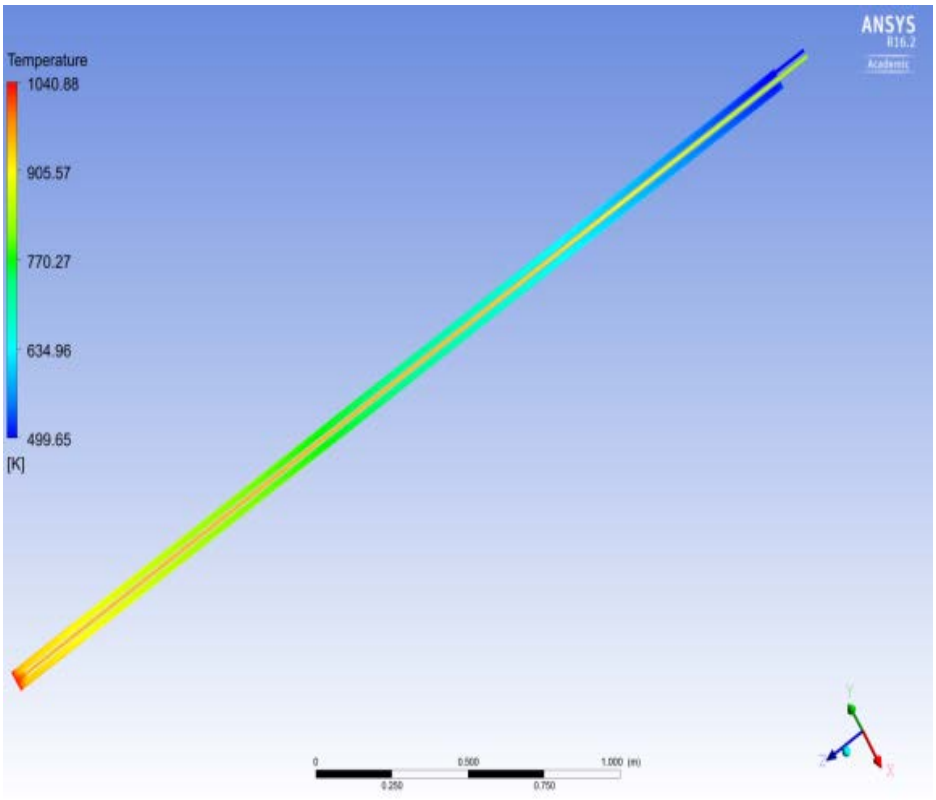

FIGURE 17. Temperature contour of the mixture in the solar tube reactor

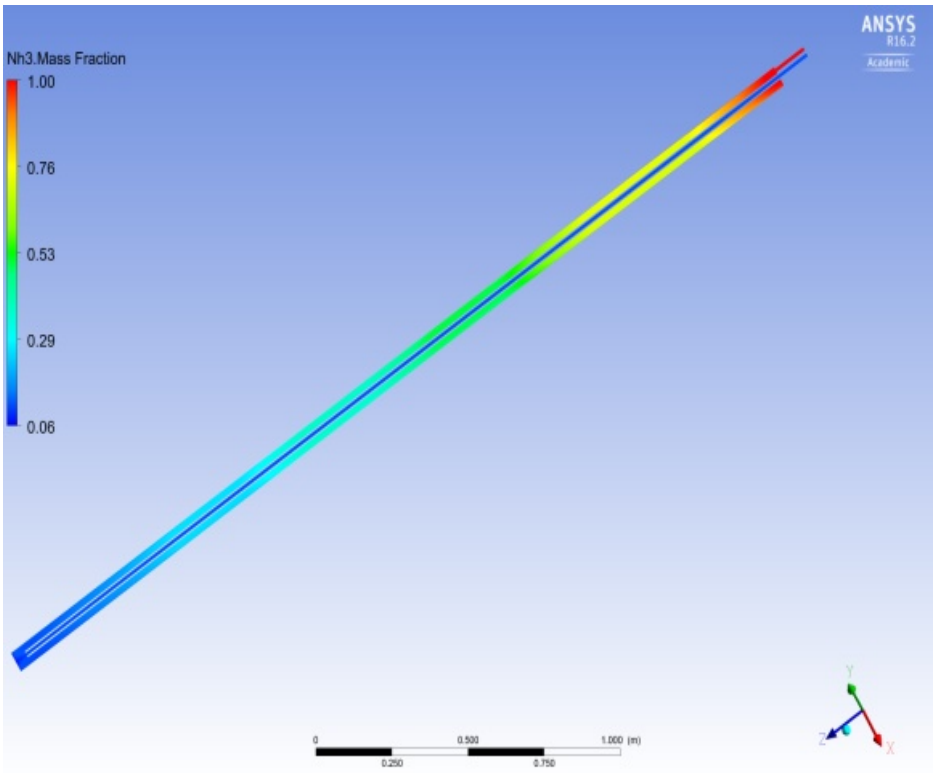

(a)

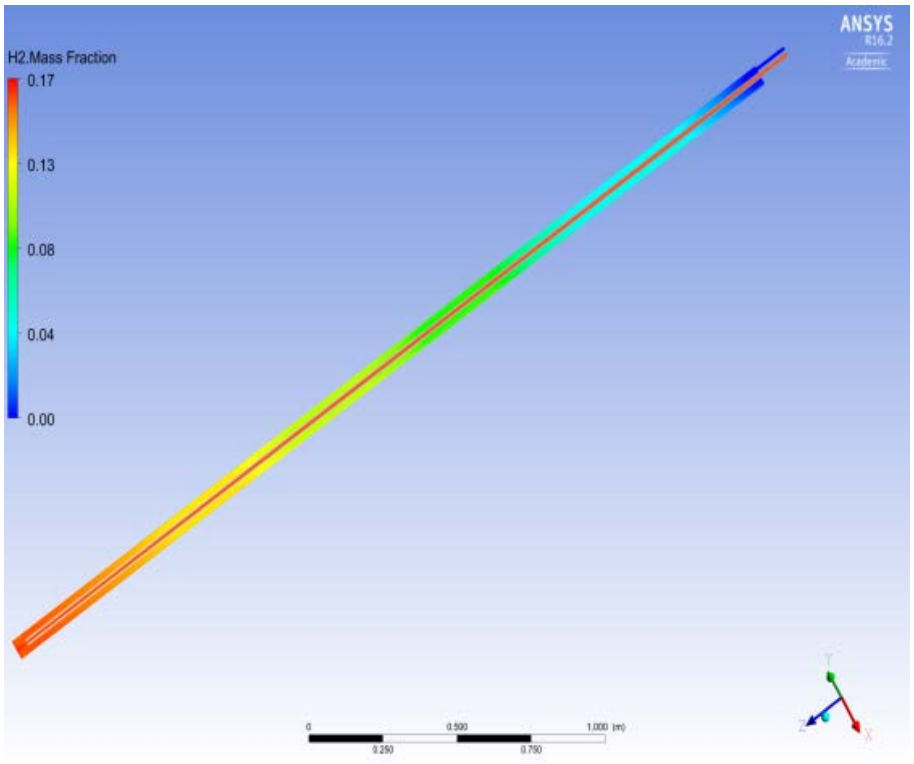

(b)

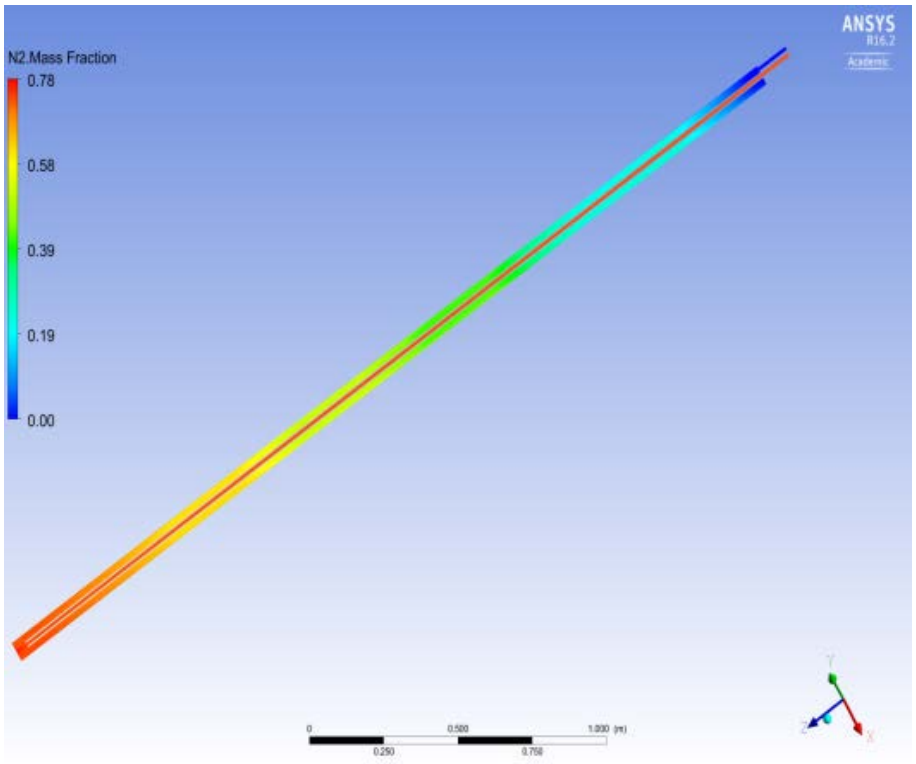

(c)

FIGURE 18. Mass concentration contours of NH3, H2, and N2 in the solar tube reactor in (a), (b), and (c) respectively

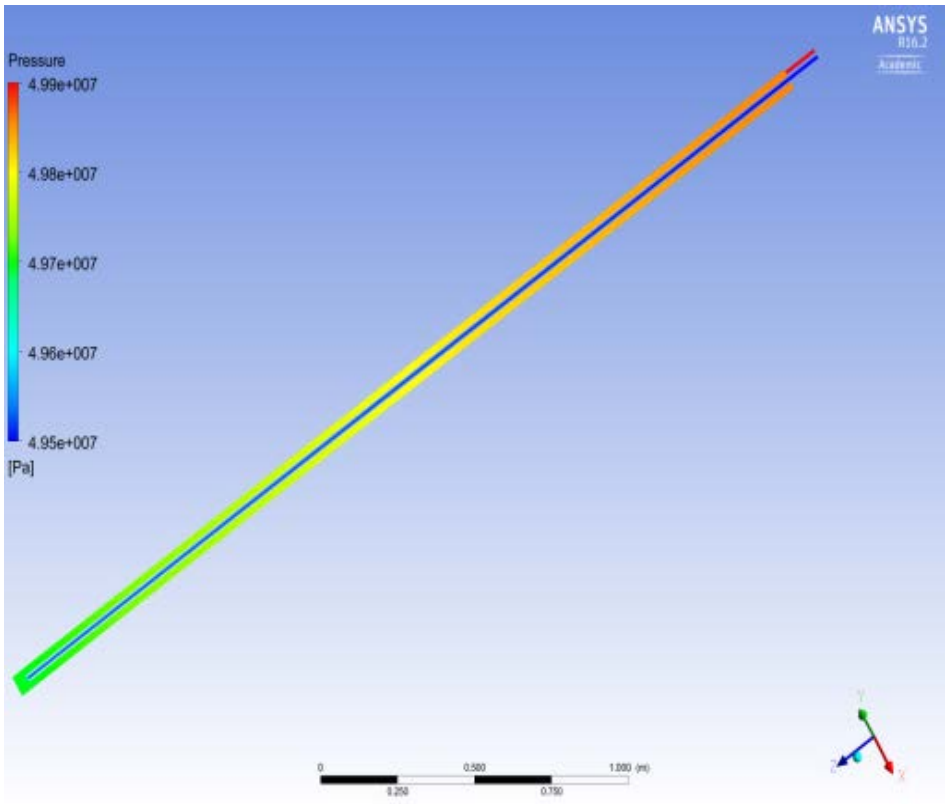

FIGURE 19. Pressure contour of the mixture in the solar tube reactor

The results from the CFD simulation are compared with the result from the MATLAB model. The geometry and boundary conditions considered are equal in both cases. Figures (20) and (21) show a good agreement in the concentrations profiles and the temperature profiles, respectively. Both the temperature and the conversion of reactants to products are high because of the constant heat flux condition on the reactor walls. Physically the rise in temperature leads to catalyst deactivation and in order to avoid the rise in temperature the ammonia must not totally dissociated.

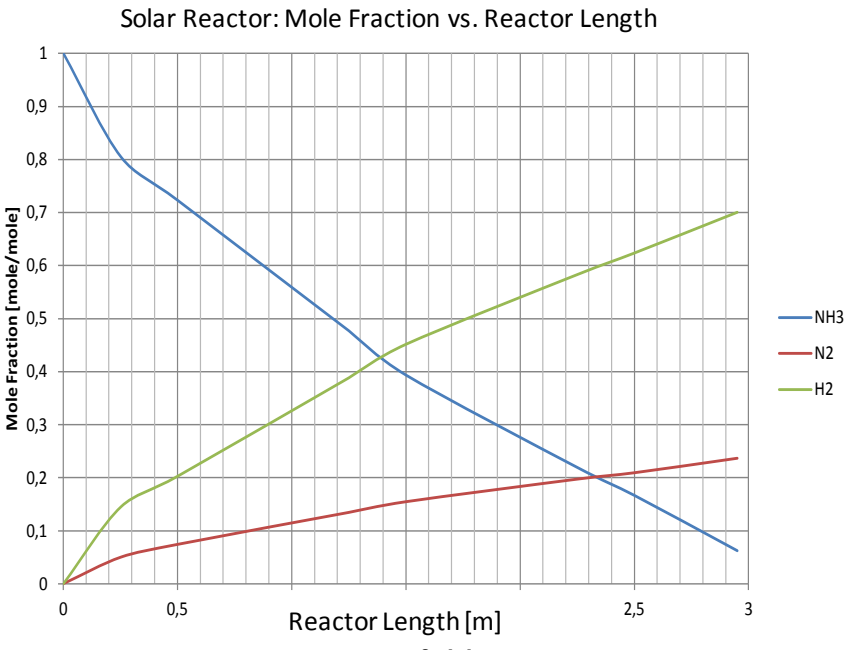

(a)

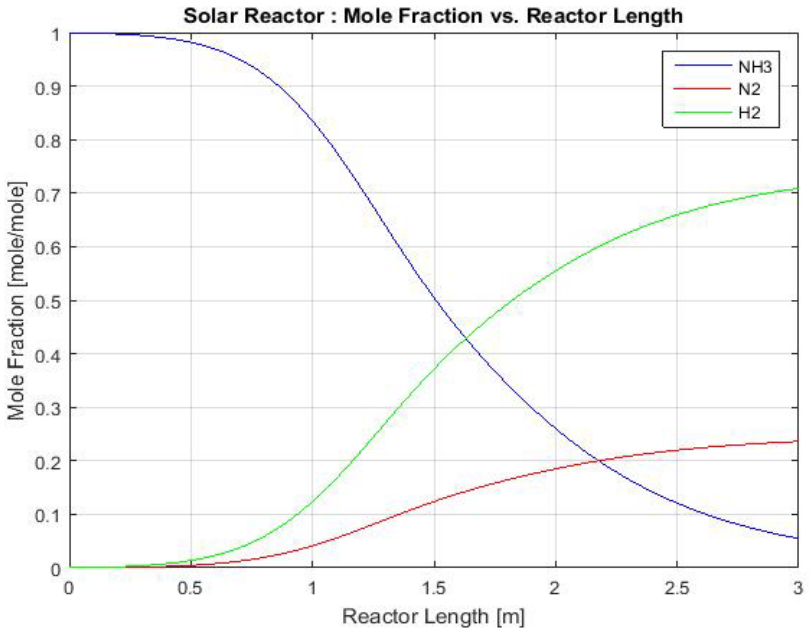

(b)

FIGURE 20. Comparison of the species' mole fractions along the solar tube reactor (a) CFD, (b) MATLAB

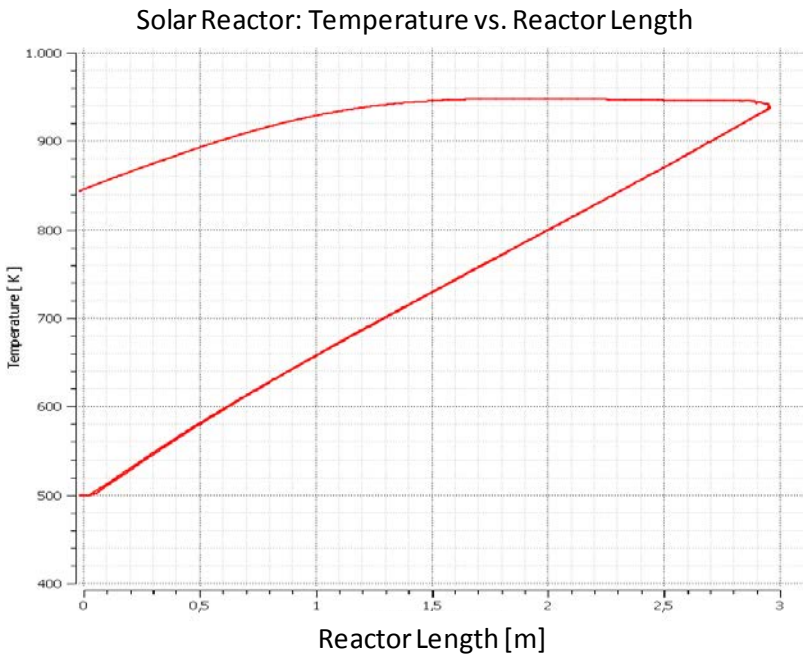

(a)

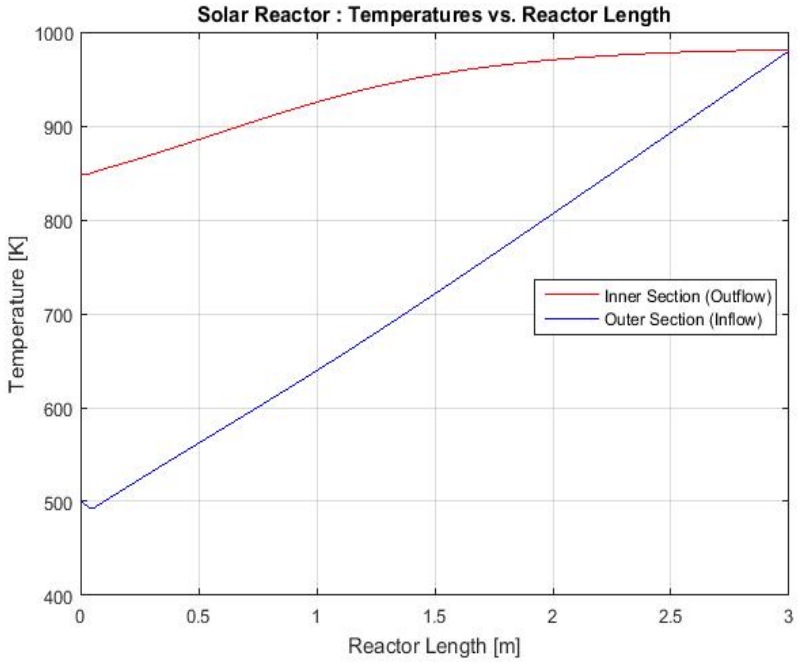

(b)

FIGURE 21. Comparison of the mixture' temperature along the solar tube reactor (a) CFD, (b) MATLAB

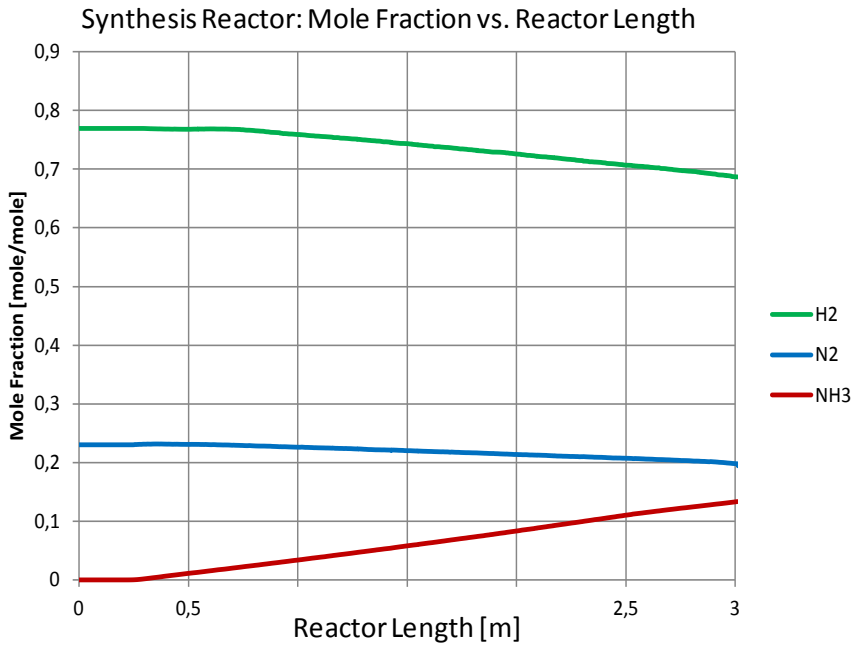

(a)

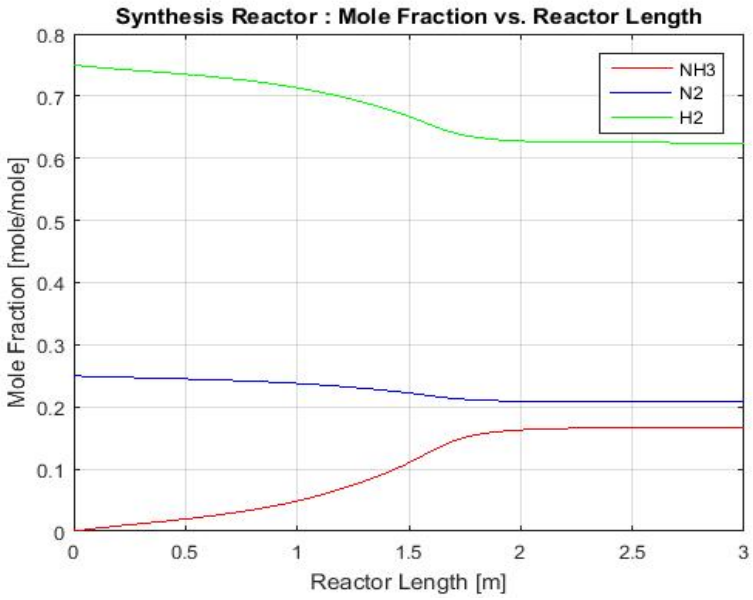

(b)

FIGURE 22. Comparison of the species' mole fractions along the synthesis tube reactor (a) CFD, (b) MATLAB

The CFD simulation results (figures 18 to 22) indicate that the concentrations of species changes due to the reaction occurring along the length of both reactors. In the solar reactor, the ammonia concentration has decreased leading the increase in the concentrations of product species (Nitrogen

and Hydrogen). In the synthesis reactor, the concentrations of reactants species (Nitrogen and Hydrogen) have decreased leading the increase in the concentration of ammonia.

The results from the CFD simulation are compared with the result from the MATLAB model. The geometry and boundary conditions are considered equal in both models. Figures (20) and (21) show good agreements in temperature and concentration profiles of the solar reactor in both models. The constant heat flux condition on the solar reactor walls makes the temperature and the conversion of reactants to products high. In the synthesis reactor there is a good agreement between the concentration profiles from both models as shown in Fig (22).

One advantage of the ammonia based close-loop storage system is that the ammonia dissociation reaction has no side reactions, making solar reactors particularly easy to control. Another is that by operating above the ambient temperature saturation pressure of ammonia, the ammonia fraction in storage is present largely as a liquid. Thus, automatic phase separation of ammonia and hydrogen/nitrogen is provided and a common storage volume can be used. Figure (23) shows the volume, pressure, mole fraction of the mixture inside the proposed vessel during a simulated 24 hours period with pressure ranging between (30 and 50) bar.

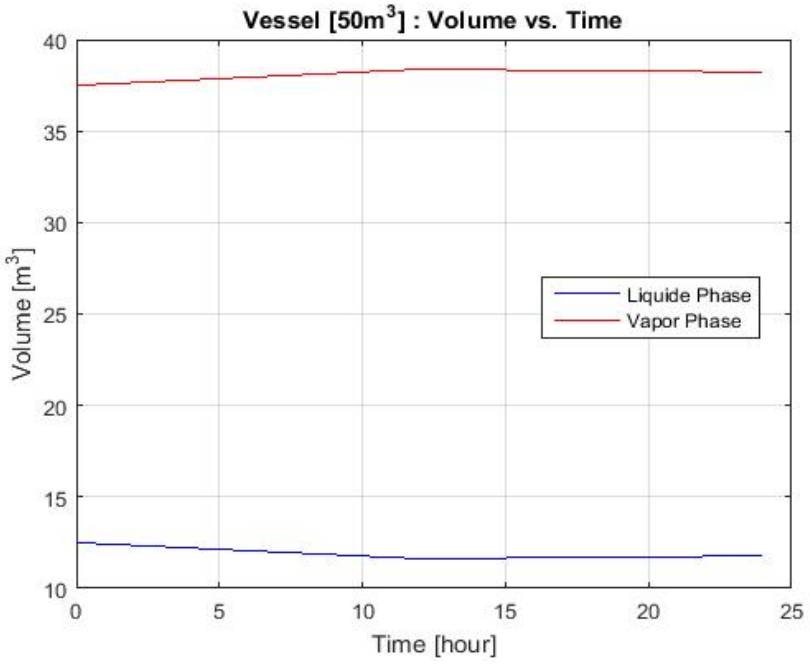

(a)

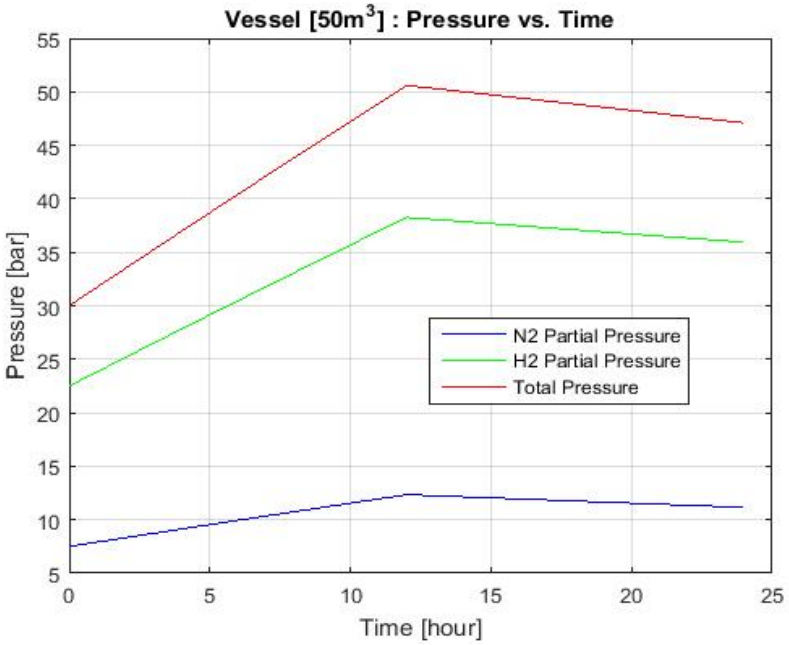

(b)

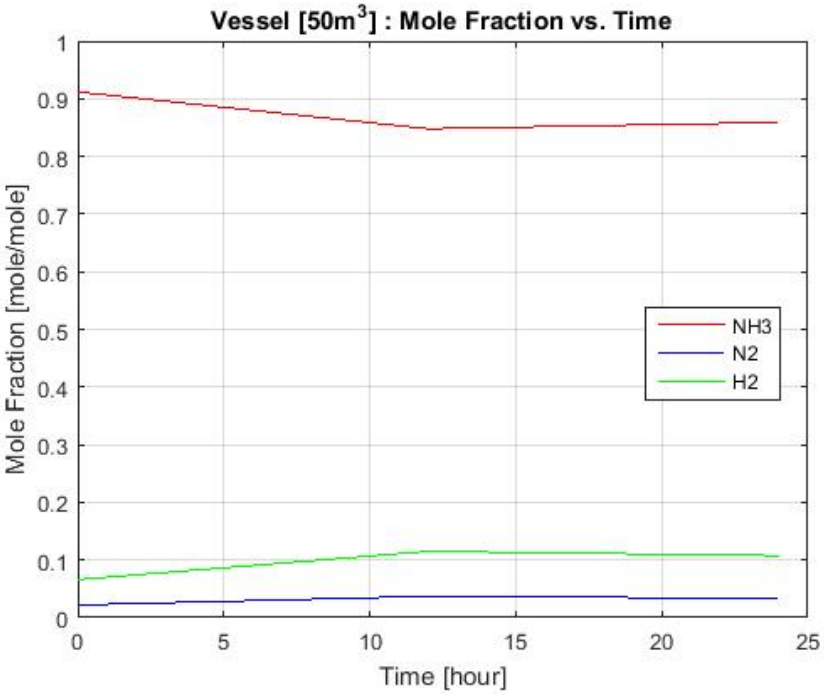

(c)

FIGURE 23. The volume, pressure, and mole fraction of gas mixture inside the proposed vessel (a), (b), and (c) respectively

Because of the effect of automatic phase separation in the common storage volume, the composition of gases sent to the heat recovery reactor for power production is independent of the degree of dissociation achieved in the solar reactors during energy storage.

To evaluate the ammonia based thermochemical energy storage system with ($50\,m^3$) vessel a comparison to state of the art thermal storage system (two-tank molten salt) is recommended. For a hypothetical ($50\,MWe$) ($110\,MWt$) plant with 12 hours of storage a rough engineering comparison between both systems can be made as shown in table (6, and 7)

TABLE 6. Commercial Two-Tank molten salt system

Thermal capacity $[MWh]$	1320
Energy $[MJ]$	4752000
Specific energy $[kJ/kg]$	450
Inventory $[tons]$	10560
Density $[kg/m^3]$	1800
Volume $[m^3]$	5867
The system in a 2-Tank arrangement is double (1 hot, 1 cold storage)	
The tanks are atmospheric (thickness 15-29 mm)	
The hot tank needs extensive insulation	

TABLE 7. Ammonia based thermochemical storage system with a VESSEL

Enthalpy of reaction $[kJ/mol]$	66.8
Molar mass of NH_3 $[g/mol]$	17.031
Density $[kg/m^3]$	614
Specific energy $[MJ/kg]$	3929
Energy density $[MJ/m^3]$	2413
Required volume for 1320 MWh $[m^3]$	2000
Realistic size of one vessel	
Diameter $[m]$	2,5
Height $[m]$	20
Volume $[m^3]$	98,2
Number of vessels	20

In the case of ammonia based thermochemical storage system, the energy density of the $N2 + 3H2$ gas mixture is ($\approx 2413\ \mathrm{MJ}/m^3$) at the proposed storage conditions of (300 K) and (50 bar), therefore roughly ($2000\ \mathrm{m}^3$) of storage volume is required. While this is comparable to the volume required for two-tank molten salt, it has the advantage of ambient temperature storage. However, the elevated pressure in the vessel results in high cost to contain the gas in conventional steel-based pressure containment systems. In the case of two-tank molten salt system, the unwanted freezing problem during operation remains as a challenge. The salt will freeze if the temperature drops below (240 ℃) and block pipes and prevent the whole system from working and to overcome this problem a complex and costly insulation must be used.

Chapter 5 – Conclusion and Future Work

In this chapter I conclude this dissertation by summarizing my contributions and discussing directions for future work.

5.1 Summary

In this dissertation, I have focused on selected aspects of a thermochemical approach to improve the competitively of CSP tower technology. In this section, I briefly review my main conclusions.

- Developing mathematical model of the tubular ammonia solar reactor and ammonia synthesis reactor allowed analyzing the performance of ammonia solar reactor and ammonia synthesis reactor and allowed making recommendation for an optimal design of the ammonia based closed-loop storage system.

- Maintaining the optimum mass flow density rate is important for achieving the maximum ammonia dissociation and formation processes which maximizes the thermal output of the system. The model leads to the statement that the change of gas inlet temperature has a minor influence on the efficiency of both reactors.

- Operating the system at higher pressure than suggested for maximum ammonia production at the synthesis would lower the thermal output of the system. In this regard, it should be mentioned that the main objective of the synthesis in the storage system is getting the maximum heat possible in the heat recovery process unlike the conventional synthesis where producing the maximum ammonia is the objective.

The study has compared a CFD simulation for a tubular packed bed reactor for the ammonia dissociation process at the receiver and the ammonia formation process at the synthesis to a MATLAB code in both reactors. The simulation includes momentum, heat and mass transfer, and chemical reactions within the catalyst particles. The good agreement between both models in regards to temperature and concentrations profiles gives confidence about the results of the MATLAB model.

5.2 Future Directions

The model presented in this work is able to provide a rather accurate description of the major phenomena governing the operation of ammonia closed-loop storage system. However, further research of a number of topics would be beneficial as listed below.

- Our results indicated the functional feasibility of the ammonia closed-loop system. However, the results are preliminary and need to be experimentally validated before deployment can be recommended.
- A detailed engineering analysis of a scaled up system should be conducted in order to evaluate the techno-economical feasibility.

- The development of new catalysts and processes should be concomitant, with the catalyst operating conditions guiding the process design, and the bottlenecks in the process steering the development of the catalyst.

- Future work may carry out a more detailed investigation on how the change in the operational load (throughput) would affect the operating conditions such as temperature, pressure, and gas distribution in the catalyst bed.

Finally, the model-based analysis in this work has only focused on the technical characteristic of the ammonia close-loop storage system. An economic assessment of the system that satisfies demands for steam production would be valuable to see if such a storage system would be economically competitive with other alternatives.

Notation

Abbreviations

CRS	Central receiver system
STR	Solar tower receiver
CFD	Computational fluid dynamics
ANU	Australian national university
NH3	Ammonia
N2	Nitrogen
H2	Hydrogen

Greek letters

ϵ	Emissivity [-]
σ	Stefan-Boltzmann constant [J /K^4 m^2 s]
α	Absorptivity [-]
μ	Dynamic viscosity [kg m^{-1} s^{-1}]
ρ	Density [kg m^{-3}]
φ	Sphericity of the cylindrical particles or pellets. [-]
ε	Porosity [-]
β_r	Temperature exponent
λ	Thermal conductivity [$W/m.K$]
ν	Kinematic viscosity [$m2/s$]

Subscripts

ab	Absorber
ap	Aperture
add	Addition
$cold$	Cold side
$drian$	Drain stream
eff	Effective
$feed$	Feed stream
g	Gas
HEx	Heat exchanger
hot	Hot side

in	Inside
out	Outside
p	Particle
rad	Radiation

Variables

A	Area [m^2]
A_r	Pre-exponential factor [j/mol]
E	Infrared energy [w]
h	Convective heat transfer coefficient [$W/m^2.K$]
H	Enthalpy [J/kg]
n	Molar flow
Y	Mole fraction
Q	Heat flux [W]
P	Pressure [bar]
T	Temperature [K]
$\dot{m}$	Mass flow rate [kg/s]
C_p	Specific heat capacity [-]
S	Entropy [J/K]
Nu	Nusselt number
Re	Reynolds number
Pr	Prandtl number
R	Universal gas constant [8313 $J/kg.mol.K$]
$Re^{"}$	Modified Reynolds number
S_p	Surface area of the particle [m^2]
V_p	Volume of the particle [m^3]
K	Permeability [m^2]
U	Superficial fluid velocity [$m\ s^{-1}$]
D_p	Sphere particle diameter [m]
E_r	Activation energy [$mol/s.cm^3.atm$]

References

[1] A. Meiers, 2004, “Solar fuels and materials”. In: Encyclopdia of Energy, Elsevier, vol.5, p 623.

[2] A. Luzzi, K. Lovegrove, 1995, "A solar thermochemical power plant using ammonia as an attractive option for greenhouse gas abatement ". In: Pergamon, pp. 317-325

[3] C. Chen, K. Lovegrove, A. Lavine; 2015, “Design an Ammonia Synthesis for Producing Supercritical Steam in the Context of Thermochemical Energy Storage”. In: ASME PowerEnergy 2015, California

[4] H. Kreetz, K. Lovegrove, 2002, “Exergy analysis of an ammonia synthesis reactor in a solar thermochemical power system”. In: Pergamon, Elsevier, Australia, pp. 187-194.

[5] R. Abdiwe, M. Haider, “A mathematical model for ammonia solar and synthesis reactors”. In: Renewables: Wind, Water, and Solar.2016, 3:12. URL: http://www.jrenewables.com/content/3/1/12.

[6] Abdiwe, R., Haider, M. 2015. “Investigations on Heat Loss in Solar Tower Receivers with Wind Speed Variation”. International Journal of Sustainable and Green Energy. Vol.4, 2015, pp. 159-165.

[7] Springer, 2010, “VDI Heat Atlas, Second Edition”. Heidelberg, Germany.

[8] Etienne Bertrand, 2015. A project work at Vienna technical university, Vienna.

[9] Francis L. Smith, Allan H. Harvey, 2007. "Avoid Common Pitfalls When Using Henry's Law", Chemical Engineering Progress (CEP), pp. 33-39

[10] © Fluent Inc. 2006-09-20

[11] Nield and A. Donald, “Convection in Porous Media”. In: Springer-Verlag, New York, 1999.

[12] Bear and Jacob, “Dynamics of Fluids in Porous Media”. In: Dover publications Inc., New York, 1988.

[13] S. Ergun, “Fluid flow through packed columns”. In: Chemical Engineering Progress, pp 89-94, 1952.

[14] M. Chen, J. Aleixo, S. Williams, “CFD Modeling of 3-Way Catalytic Converters with Detailed Catalytic Surface Reaction Mechanism”. In: DCL International Inc, 2004.

[15] Andre Bakker, 2006 “Modeling Chemical Reactions with CFD”

Paper I

Abdiwe, R., Haider, M. (2017)

“Design of an ammonia closed-loop storage system in a CSP power plant with a power tower cavity receiver”

American Institute of Physics

Paper Π

Abdiwe, R., Haider, M. (2016)

“A mathematical model for ammonia solar and synthesis reactors”

Renewables: Wind, Water, and Solar

Paper III

Abdiwe, R., Haider, M. (2015)

“Investigation on the exergy performance of a central receiver power plant”

Fundamentals of Renewable Energy

(The extended version is included in the Appendix)

Paper IV

Abdiwe, R., Haider, M. (2015)

“Investigations on heat loss in solar tower receivers with wind speed variation”

International Journal of Sustainable and Green Energy

Appendix

Investigation on the Exergy Performance of a Central Receiver Power Plant

1. Abstract

The present paper describes the exergy analysis of a Central Receiver System (CRS) power plant. The plant consists of a thousand heliostats with an area of 130 m^2 each, an external receiver with an area of 59 m^2 and a height of 70 m , a steam generator, two steam turbines with a reheater in between, two feed water heaters and a condenser. EBSILON®Professional software was used to obtain the exergy efficiency and the irreversibility in each component of the power plant to pinpoint the causes and locations of the thermodynamic imperfection. The model analyzed and tested the effect of two design parameters including the Direct Normal Irradiation (DNI) and the outlet temperature of the Heat Transfer Fluid (HTF) on the exergy performance. The obtained results show at a constant DNI the maximum exergy loss occurs at the Receiver followed by the heliostat field and the power cycle has the lowest exergy loss. The increase of the DNI affects negatively the exergy efficiency of the overall system. The variation of the outlet temperature of the HTF has an impact of the exergy performance of the receiver subsystem as well as the overall system; the increase of the outlet temperature from 450 $^{\circ}C$ to 600 $^{\circ}C$ leads to an increase the exergy efficiency of the receiver to about 5% and an increase the exergy efficiency of the overall system to about 1%.

Keywords: Central Receiver System, External receiver, Exergy efficiency, Irreversibility

2. Nomenclature

η_{II}	Exergy efficiency (%)
W_{net}	Net output of the overall system (W)
$\mathrm{W_{turbine}}$	Output of both turbines (W)
W_{pump}	Work for both pumps (W)
y & z	Mass fractions
m_{st}	Steam mass flow rate (kg/s)
m_{ms}	Molten salt mass flow rate (kg/s)
T_o	Atmospheric temperature ($^{\circ}C$)
T_{wi}	Inlet water at the condenser ($^{\circ}C$)
$T_{rec,sur}$	Receiver surface temperature ($^{\circ}C$)
I_{total}	Overall system irreversibility (W)
$I_{heliostat}$	Heliostat field irreversibility (W)
$I_{receiver}$	Receiver irreversibility (W)
I_{pcycle}	Power cycle irreversibility (W)
Q^*_{total}	Total isolation (W)
Q^*_{inc}	Incident isolation (W)
$Q_{inc,abs}$	Heat absorbed by the receiver (W)
$Q_{inc,loss}$	Heat lost at the receiver (W)
ψ^*_{total}	Exergy input into the heliostat field (W)
ψ^*_{inc}	Exergy delivered to the receiver (W)
$\psi_{inc,abs}$	Exergy absorbed by the receiver (W)

3. Introduction

Solar energy is an important alternative energy source used in many applications, especially in solar power systems which utilize the heat generated by collectors concentrating and absorbing the sun's energy to drive heat engines/generators and produce electric power [1]. Most known types of the solar-thermal systems to produce electricity are trough/steam turbine, tower/steam turbine, and dish/heat engine systems. Out of all these technologies, tower/steam turbine looks like to be the best choice for high power production as it has the largest operating temperature range [2]. Tower/steam turbine or what so called Central Receiver System (CRS) is composed of the following main components: the heliostats, the receiver and the power block. The thermal storage and balance of plant components allow high temperatures which lead to high efficiency of the power conversion system [3]. However, the power generation efficiency of the CRS systems is found to be low which directly increase the capital cost of the electricity generation. To investigate the cause of the low generation efficiency in the power generation system an exergy analysis is required. The exergy analysis has proven to be a powerful tool in thermodynamic analyses of the system [4]. Therefore, a theoretical investigation based on the second law efficiency has been conducted for a CRS power plant.

The Exergy is the maximum useful work that can be obtained from a system at a given state in a given environment; in other words, the most work you can get out of a system. In the last several decades exergy analysis has begun to be used for system optimization by analyzing the exergy destroyed in each component in a process. With the exergy analysis we can see where we should be focusing our efforts to improve system efficiency. The exergy analysis method is a useful tool for promoting the goal of more efficient energy-resource use, as it enables the locations, types and true magnitudes of wastes and losses [5].

However, few papers have appeared on the exergy analysis and performance assessment of the solar thermal power plant. Bejan (1981) showed that the amount of useful energy (exergy) delivered by solar collector systems is affected by heat transfer irreversibility occurring between the sun and the collector, between the collector and the ambient air, and inside the collector [6]. Singh (2000) stated that the collector-receiver assembly is the part where the losses are maximum and the maximum exergy loss occurs in the solar collector field [7]. Gupta and Kaushik (2010) made an exergy analysis for the different components of a proposed conceptual direct steam generation (DSG) solar–thermal power plant and found that the maximum exergy loss is in the solar collector field while in other plant components it is small [5]. Chao Xu (2011) evaluated the exergy losses in each component and in a power tower solar plant and the results showed that the maximum exergy loss occurs in the receiver system [8].

The objective of this paper is to evaluate the exergy efficiencies and the irreversibilities of all components of a CRS power plant with an external central receiver and a supercritical Rankine cycle and pinpoint the causes and locations of the thermodynamic imperfection and the magnitude of the process irreversibilities in the system. Two parameters have been varied to see their effect on the exergy efficiency of the receiver and the overall system.

4. System Configuration

The schematic of the solar tower power plant is shown in figure (1). The system consists of a heliostat field system, an external central receiver, a steam generator, two steam turbines with a reheat in between, a wet condenser, open and close feed water heaters and two pumps.

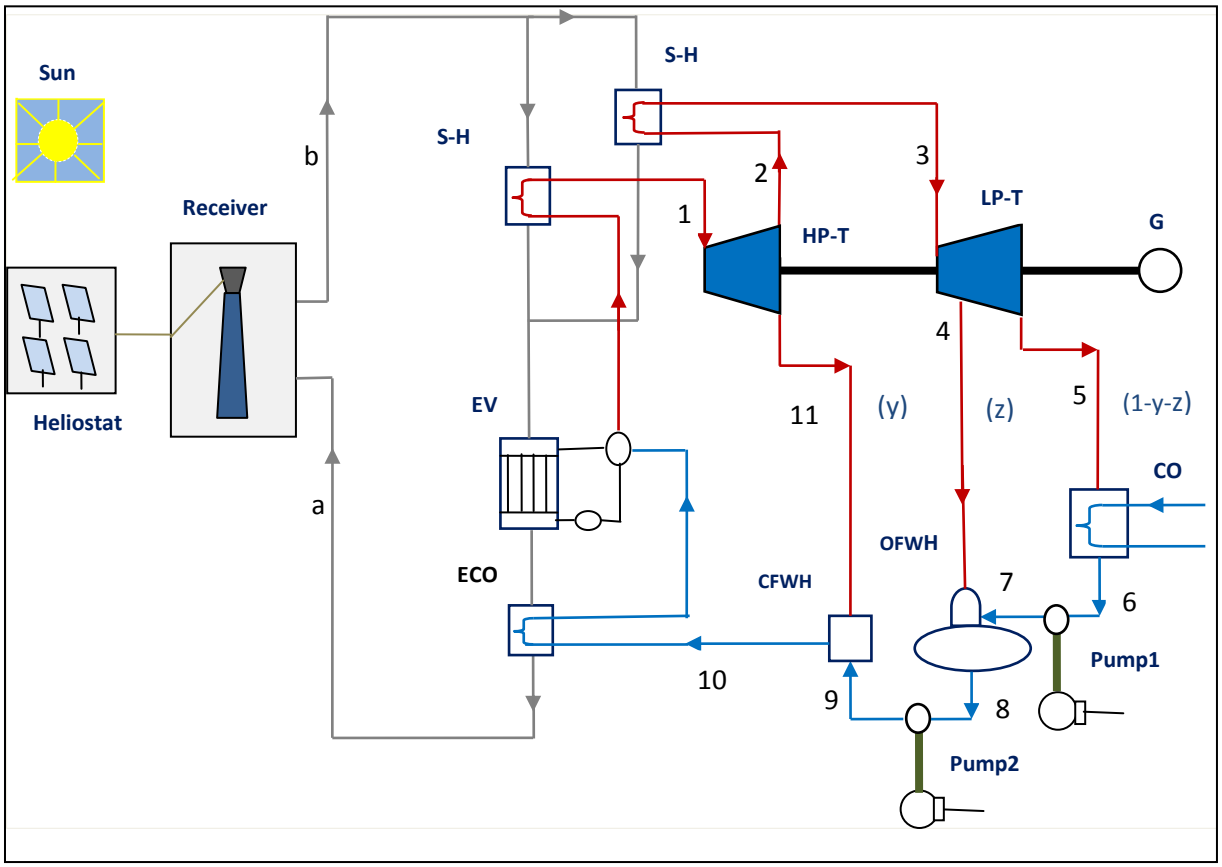

FIGURE 1. The schematic diagram of the system layout

The target is to do an exergy analysis for each component of the power plant including the power cycle, the receiver and the heliostat to have more profound understanding of the performance of the CRS power plant. Also to compare all components and see which one has the biggest fractional exergy loss which will provide the guides of improving the performance and optimizing the operation.

The following assumptions are made in the analysis:

a. The system runs of steady state with a constant solar insulation
b. Capacity of the power plant is 30 MW
c. The CRS power plant is using molten salt as HTF
d. The temperature of molten salt entering the receiver 290 $^{\circ}C$ and leaving it 565 $^{\circ}C$.
e. Kinetic and potential exergy are ignored
f. The optical efficiency of the receiver is assumed to be 93%
g. Conductive heat loss in the receiver is ignored

5. The Exergy Analysis

The Second Law Efficiency or what so called the exergy efficiency of the whole system can be defined as the ratio of net electricity output from the whole system to the exergy input associated with the solar irradiation on the heliostat surface [8]. The exergy input into the heliostat field (ψ^{*}_{total}) is basically the electricity output (W_{net}) plus the irreversibility (I_{total}) which is also called the exergy destroyed. The exergy destroyed represents energy that could have been converted into work but was instead wasted. Therefore, the exergy efficiency of the overall system is given by:

$$\eta_{II} = \frac{W_{net}}{\psi^{*}_{total}} \qquad (1)$$

$$\eta_{II} = \frac{W_{net}}{(W_{net}+I_{total})} \qquad (2)$$

Where the net output work (electricity) from the whole system is calculated as:

$$W_{net} = W_{hptur} + W_{lptur} - W_{pump1} - W_{pump2} \qquad (3)$$

The total irreversibility (I_{total}) of the whole system is the summation of the irreversibilities of the subsystems:

$$I_{total} = I_{heliostat} + I_{receiver} + I_{pcycle} \qquad (4)$$

5.1 Power cycle

To improve the exergy efficiency of the power cycle a regenerative Rankine cycle is used as the case of most existed solar tower power plants. The power cycle of our system as shown in figure (1) consists of high and low-pressure turbine stages, a condenser, two pumps and feed water heater. Since a molten salt is being used as Heat Transfer Fluid, it is necessary to use an open and a closed feed water heaters to prevent the solidification of the molten salt in the steam generation subsystem.
The exergy efficiency of the power cycle subsystem can be calculated as:

$$\eta_{II} = \frac{W_{net}}{W_{net}+I_{pcycle}} \qquad (5)$$

$$W_{net} = W_{turbine} - W_{pump} \qquad (6)$$

$$W_{turbine} = W_{hptur} + W_{lptur} \qquad (7)$$

$$W_{pump} = W_{pump1} + W_{pump2} \qquad (8)$$

In order to calculate the power cycle output (W_{net}) , it is necessary to apply an energy balance in the regenerative Rankine cycle. As a result the power delivered by the turbines and consumed by the pumps can be evaluated as following:

$$W_{turbine} = [(h_1 - h_2) + (1-y)(h_3 - h_4) + (1-y-z)(h_4 - h_5)] \qquad (9)$$

$$W_{pump} = (1-y-z)(h_7 - h_6) + (1-y)(h_9 - h_8) \qquad (10)$$

y & z are the mass fractions and can be calculated by applying an energy balance on the open and the closed feed water heaters. Therefore, the values of the mass fractions are:

$$y = \frac{h_{10}-h_9}{h_2-h_9} \qquad (11)$$

$$z = \frac{(1-y)(h_8-h_7)}{(h_4-h_7)} \qquad (12)$$

The irreversibility of the power cycle (I_{pcycle}) is the summation of the irreversibility of each component of the power cycle subsystem.

$$I_{pcycle} = I_{turbines} + I_{condenser} + I_{sgenerator} + I_{pump1} + I_{pump2} + I_{ofwh} + I_{cfwh} \qquad (13)$$

The entropy generation in a system is the cause of the exergy destruction. The destruction of useful work because of the entropy generated is knowing also as irreversibility. The exergy destruction is a

proportional of the entropy generated. The general equation for the exergy destruction can be expressed as:

$$I = T_o S_{gen} \qquad (14)$$

S_{gen} is the entropy generated, for a steady state control volume, this leads us to:

$$S_{gen} = \sum_{out} m_e s_e - \sum_{in} m_i s_i - \sum \frac{Q}{T_k} \qquad (15)$$

Where

m_i & m_e are the mass flow rate in and out respectively

s_i & s_e are the entropy in and out respectively

Q is the heat loss to the surrounding.

T_k is the temperature of the heat source.

As a result, the irreversibility of each component of the power cycle can be defined as:

$$I_{turbines} = m_{st} T_o [(s_2 - s_1) + (1 - y)(s_4 - s_3) + (1 - y - z)(s_5 - s_4)] \qquad (16)$$

$$I_{sgenerator} = m_{st} T_o \big((s_1 - s_{10}) + (1 - y)(s_3 - s_2) - (((h_1 - h_{10}) + (1 - y)(h_3 - h_2))/ T_{rec,sur})\big) \qquad (17)$$

$$I_{pump} = I_{pump1} + I_{pump2} \qquad (18)$$

$$I_{pump} = m_{st} T_o (1 - y - z)(s_7 - s_6) + m_{st} T_o (1 - y)(s_9 - s_8) \qquad (19)$$

$$I_{ofwh} = m_{st} T_o \big((1 - y)s_8 - z s_4 - (1 - y - z)s_7\big) \qquad (20)$$

$$I_{cfwh} = m_{st} T_o \big(y s_2 + (1 - y)(s_{10} - s_9)\big) \qquad (21)$$

$$I_{condenser} = m_{st} T_o (1 - y - z)((s_6 - s_5) - \left(\frac{h_6 - h_5}{T_{wi}}\right)) \qquad (22)$$

5.2 Receiver

In the solar receiver, the heat flux arriving at the aperture area is transferred into a heat flow directed to the HTF. The heat is used to raise the temperature of theHTF. On the way from the aperture to the fluid, some optical and thermal losses occur. Therefore, the incident isolation can be obtained by:

$$Q^{*}_{inc} = Q_{inc,abs} + Q_{inc,loss} \qquad (23)$$

$$Q_{inc,abs} = m_{ms}(h_b - h_a) \qquad (24)$$

h_a & h_b are the inlet and exit enthalpy of the molten slat at the receiver respectively.

Regarding the thermal losses, only the radiation and convective losses have been considered and the others are partially small and to be ignored.

$$Q_{inc,loss} = Q_{loss,radiation} + Q_{loss,convection} + Q_{loss,optical} \qquad (25)$$

The radiation and convective heat loss is obtain from a CFD model for the same receiver geometry and same boundary conditions done by the author [9]. Table (1) shows the values of the thermal heat loss at the receiver.

Table 1. Thermal loss at the receiver [9]

DNI [W/m^2]	Wind speed [m/s]	Radiation loss [kW]	Convection loss [kW]
800	4	774	251

The optical efficiency is assumed to be 93% . Therefore, the $Q_{loss,optical}$ is equal to $0{,}07Q^{*}_{inc}$

The exergy delivered to the receiver can be calculated by [8]:

$$\psi^{*}_{inc} = Q^{*}_{inc}\left(1 - \frac{T_o}{T^{*}}\right) \qquad (26)$$

T^{*} is the apparent sun temperature as an exergy source and will considered $4500\ K$.

Similarly the exergy absorbed in the receiver can be given by:

$$\psi_{inc,abs} = Q_{inc,abs}\left(1 - \frac{T_o}{T_{rec,sur}}\right) \qquad (27)$$

The exergy efficiency of the receiver is defined as

$$\eta_{II} = \frac{\psi_{inc,abs}}{\psi^*_{inc}} \qquad (28)$$

The irreversibility in the receiver

$$I_{receiver} = \psi^*_{inc} - \psi_{inc,abs} \qquad (29)$$

5.3 Heliostat field system

The incoming solar irradiance onto the receiver aperture area is concentrated by a large number of individually tracked heliostats. The flux density distribution on a defined aperture surface is the output of the heliostat field. This aperture surface can be used as an interface between the optical concentrator and the solar receiver.

The total isolation (Q^*_{total}) is a proportional to the heliostat field aperture area and can be given by [8]:

$$Q^*_{total} = A_h . DNI \qquad (30)$$

A_h is the heliostat field aperture area.

DNI is the direct normal irradiation.

$$Q^*_{total} = Q^*_{inc} + Q^*_{loss} \qquad (31)$$

The total exergy (ψ^*_{total})associated with the solar irradiation on the heliostat mirror surface (Q^*_{total}) can be expressed as [8]:

$$\psi^*_{total} = Q^*_{total}\left(1 - \frac{T_o}{T^*}\right) \qquad (32)$$

$$\psi^*_{total} = \psi_{inc} + I_{heliostat} \qquad (33)$$

The exergy efficiency of the heliostat will be as:

$$\eta_{II} = \frac{\psi^*_{inc}}{\psi^*_{total}} \qquad (34)$$

The irreversibility in the heliostat is:

$$I_{heliostat} = \psi^*_{total} - \psi^*_{inc} \qquad (35)$$

6. Fractional Exergy Loss

The ratio of the irreversibility of each component to the irreversibility of the whole system is the fractional exergy loss for that component. That illustrates the loss of useful energy in each component which helps us to decide where we should be focusing our efforts to improve system efficiency.
The fractional exergy loss of each component can be calculated as:

$$\text{Fractional Exegy Loss}_{\text{componant}} = \frac{\text{I}_{\text{componant}}}{\sum \text{I}_{\text{total}}} \times 100 \qquad (36)$$

7. Results

The exergy analysis has been carried out for a CRS power plant with reheat-regenerative Rankine cycle using one open and closed feed water heater. At a constant DNI the exergy efficiency differs from a component to another. The highest exergy efficiency is associated with the power cycle subsystem meanwhile the receiver subsystem has the lowest exergy analysis. It can be seen from the graph in the figure (2) that at fixed DNI $800\,W/m^2$ and also fixed Outlet temperature of the HTF (molten salt) $565\ ^{\circ}C$, the exergy efficiencies are 80%, 74% and 58% for the power cycle, the heliostat and the receiver respectively.

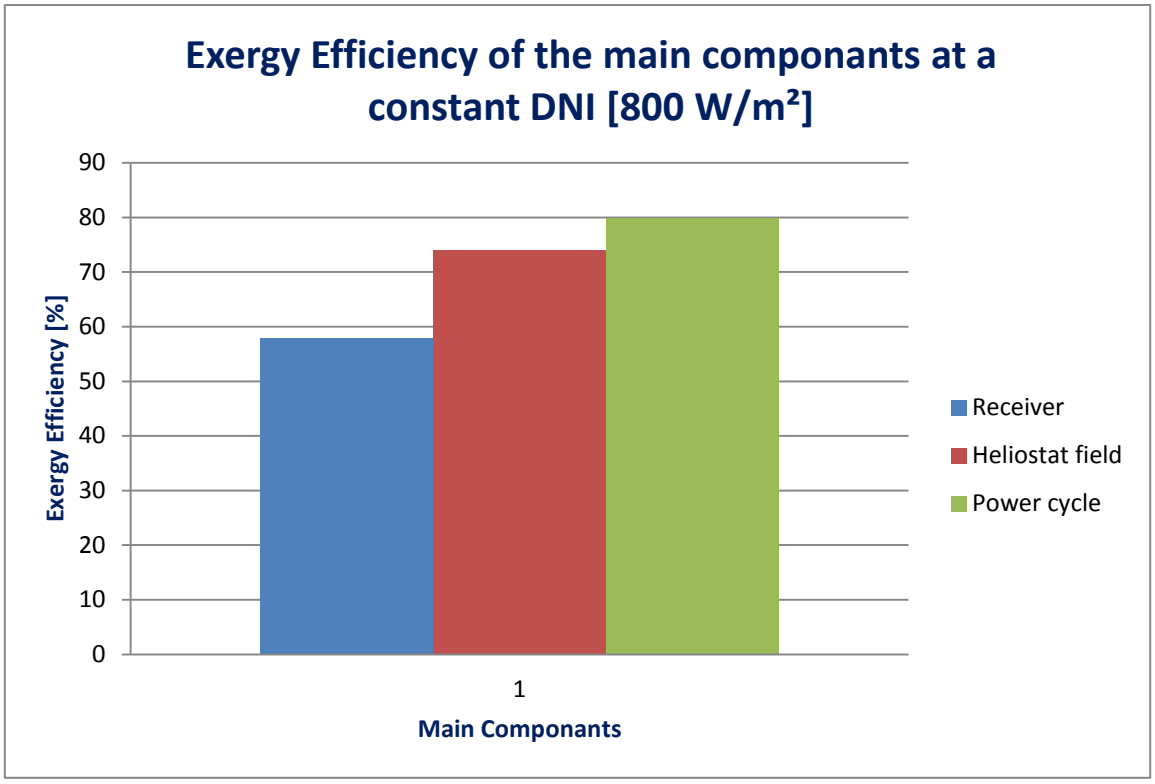

FIGURE 2. The comparison of the exergy efficiency of the main components in the system

Figure (3) illustrates the effect of the DNI on the fractional exergy loss. The fractional loss at each component of the power cycle subsystem decreases slightly with the increase of the DNI. However, at the receiver and the heliostat field subsystems the case is opposite. The fractional loss at the receiver and the heliostat field increases with the increase the DNI and as a result the exergy efficiency in both subsystems decreases.

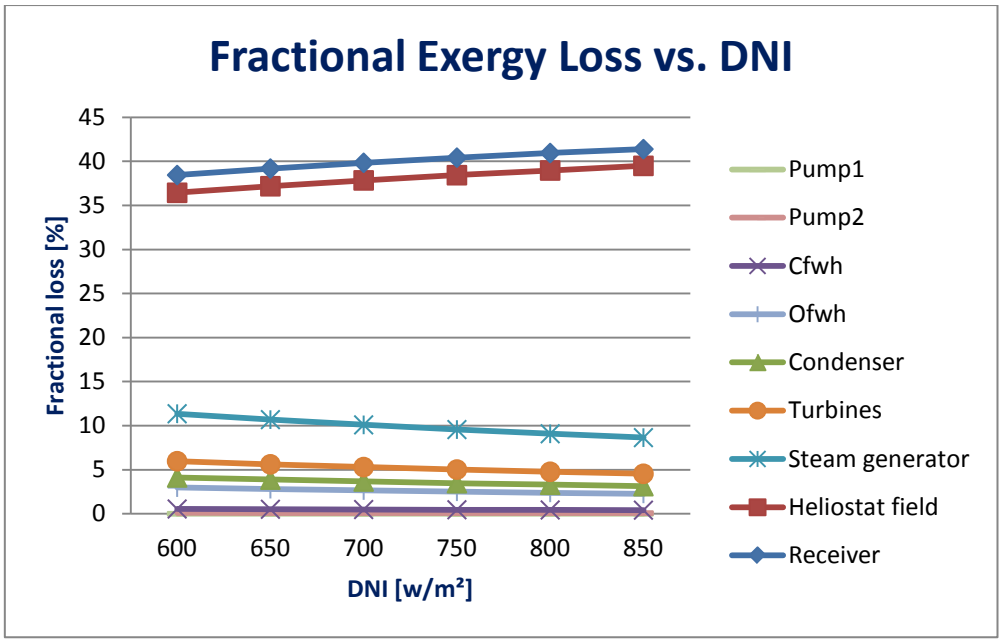

FIGURE 3. The effect of the direct normal irradiation on the fractional exergy loss of all components

The total isolation (Q^*_{total}) at the heliostat field and the exergy (ψ^*_{total}) associated with it are both a proportional of the DNI as illustrated in equations (30) and(32). However, the second law efficiency of the heliostats ($\eta_{II,heliosat}$) is inversely proportional of the DNI and it gets lower because the irreversibility of the heliostat gets higher as shown in equation(34). Similarly when the DNI increase the exergy delivered to the receiver (ψ^*_{inc}) increase and also the irreversibility at the receiver increase ($I_{receiver}$) and this leads to the decrease in the exergy efficiency of the receiver ($\eta_{II,receiver}$) as described in the equation (28).

Figure (4) shows the effect of the DNI on the exergy efficiency of the whole system. Since the irreversibilities at the receiver and the heliostat field increase with the increase of the DNI, the total irreversibility (I_{total}) increases and as a result the exergy efficiency of the whole system decreases.

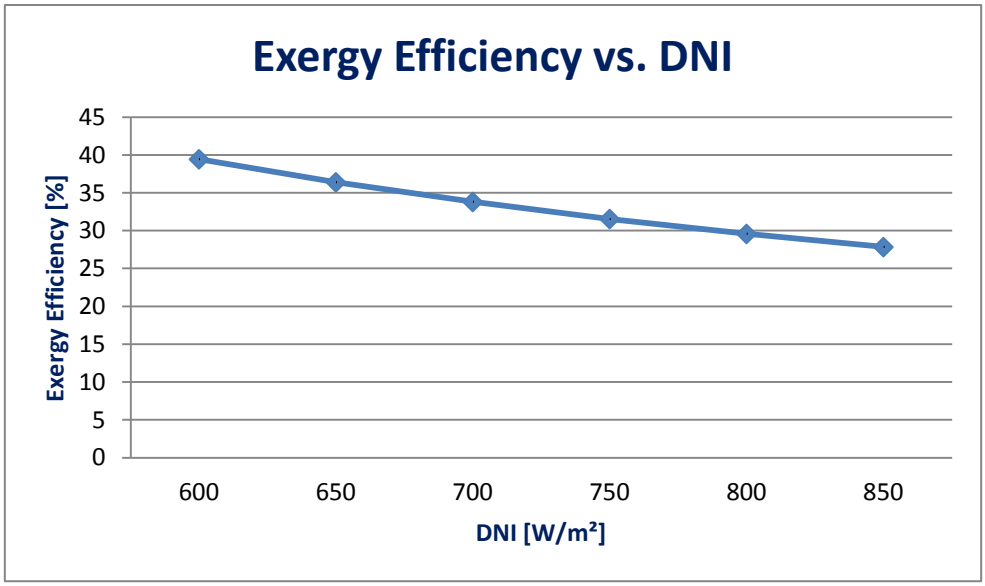

FIGURE 4. The effect of the DNI values on the exergy efficiency of the system

The variation in the exergy efficiency of both the receiver and the overall system with the outlet temperature of the molten salt is shown in the figure(5). It can be seen that the exergy efficiency at the receiver and the overall system both increase to a certain degree with the increase of the outlet temperature. The outlet temperature has more effect on the exergy efficiency of the receiver subsystem with comparison to the overall system. The increase of the outlet temperature of the molten salt from 450 ˚C to 600 ˚C will lead to an increase in exergy efficiency at the receiver to about 5% while the increase of the exergy efficiency at the overall system is only in the range of1%.

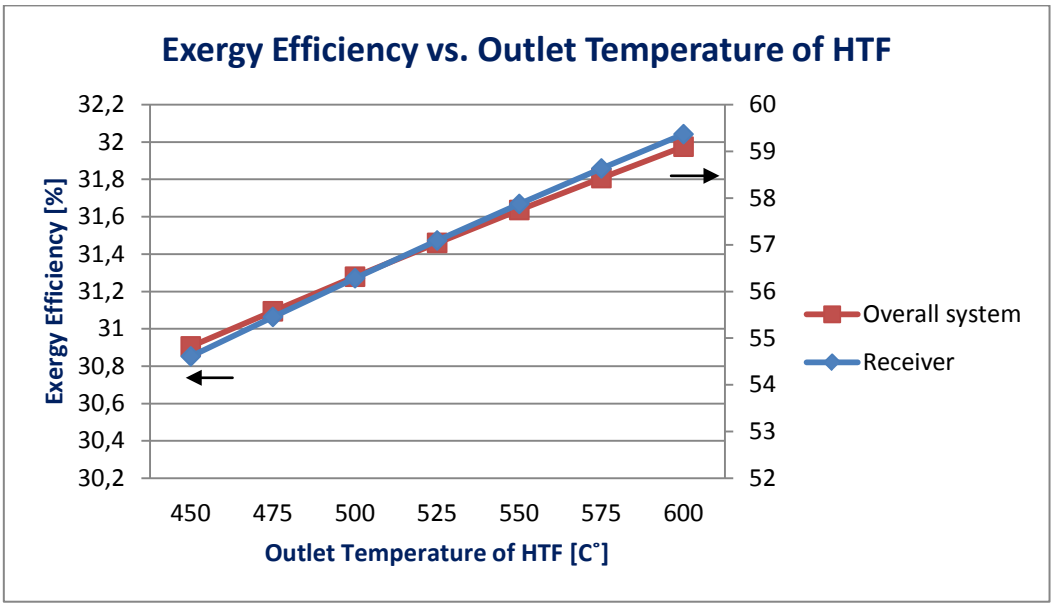

FIGURE 5. The effect of outlet temperature of the HTF (molten salt) on the exergy efficiency of the receiver and the whole system**.**

The fractional exergy loss at the receiver and the heliostat subsystems varies with different values of the outlet temperature as shown in figure (6). Regarding the receiver subsystem the fractional exergy loss decreases with the increase of the outlet temperature. However, the fractional exergy loss at the heliostat field subsystem increases and this lowers the exergy efficiency. As the outlet temperature of the molten salt gets higher the flow rate should be lowered in order to heat the molten salt to the required temperature and therefore, the absorbed heat at the receiver by the molten salt ($Q_{inc,abs}$) is diminishing. As shown in equation (27) the exergy delivered to the receiver ($\psi_{inc,abs}$) is proportional of the absorbed heat by the receiver ($Q_{inc,abs}$). Therefore, the exergy delivered to the receiver ($\psi_{inc,abs}$) reduced and as a result the exergy efficiency of the receiver decreases as illustrated in equation (28). It can be also seen from the figure (6) that the variation of the outlet temperature of the molten salt has no effect on the exergy efficiency of the power cycle subsystem components.

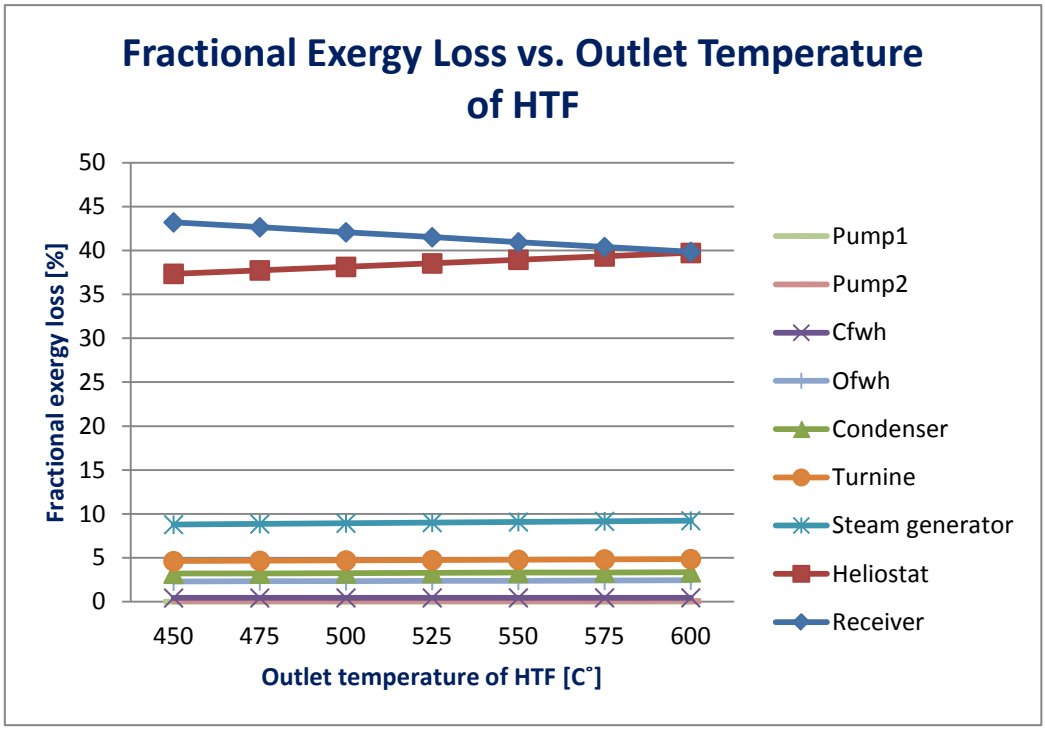

FIGURE 6. The effect of the outlet temperature of the HTF (molten salt) on the fractional exergy loss of all the components in the system

8. Conclusions

In this paper, a theoretical investigation based on the second law efficiency has been conducted for a CRS power plant with an external central receiver and a supercritical Rankine cycle to pinpoint the causes and locations of the thermodynamic imperfection and the magnitude of the process irreversibilities in the system. The following conclusions can be drawn from study:

- The receiver subsystem has the highest fractional exergy loss and as a result it has the lowest exergy efficiency (58%) followed by the heliostat field subsystem(74%). While the power cycle subsystem has the lower fractional exergy loss and as result the highest exergy efficiency (80%).
- The variation of the DNI affects the fractional exergy loss in all components. The increase of the DNI leads to a decrease of the fractional exergy loss in the power cycle subsystem components and an increase of the fractional exergy loss in the receiver and heliostat field subsystems. As result the increase of the DNI affects negatively the exergy efficiency of the overall system.
- The variation of the outlet temperature of the HTF (molten salt) has no significant impact on the exergy efficiency of the receiver subsystem as well as the overall system. It is found that by increasing the outlet temperature of the molten salt from $450\,^{\circ}C$ to $600\,^{\circ}C$ will increase the exergy efficiency of the receiver subsystem to almost 5% and almost 1% to the exergy efficiency of the overall system.

9. Acknowledgements

The author wish to thank the institute for Energy Systems and Thermodynamics at Vienna University of Technology(TU). I am also grateful to Professor Haider for the help provided in guiding the study.

10. References

[1] L.Ya-Qi, H. Ya-Ling, W. Zhi-Feng, 2012, “Exergy analysis of two phase change materials storage system for solar thermal power with finite-time thermodynamics”. In: Renewable Energy, Chine, pp. 447-454.

[2] T.A.H. Ratlamwala, I. Dincer, M. Aydin, 2012, “Energy and exergy analyses and optimization study of an integrated solar heliostat field system for hydrogen production”. In: International Journal of Hydrogen Energy, Turkey, pp. 18704-18712.

[3] IRENA, 2012, "Concentrating Solar Power. Cost analysis series". In: Renewable Energy Technologies.

[4] A. Hepbasli, 2008, “A key review on exergetic analysis and assessment of renewable energy resources for a sustainable future”. In: Renewable and Sustainable Energy Reviews, Turkey, pp. 593-661.

[5] M.K. Gupta, S.C. Kaushik, 2010, “Exergy analysis and investigation for various feed water heaters of direct steam generation solar–thermal power plant”. In: Renewable Energy, India, pp. 1228–1235.

[6] A. Bejan, D.W. Kearney, F. Kreith, 1981, “Second law analysis and synthesis of solar collector systems”. In: Solar Energy Engineering, pp. 23-28.

[7] N. Singh, S.C. Kaushik, R.D. Misra, 2000, “Exergetic analysis of a solar thermal power system”. In: Renewable Energy, India, pp. 135-143.

[8] Xu. Chao, W. Zhifeng, Li. Xin, S. Feihu, 2011, “Energy and exergy analysis of solar power tower plants”. In: Applied Thermal Engineering, China, pp. 3904-3913.

[9] R. Abdiwe, 2015, “Investigations on heat loss in solar tower receivers with wind speed variation”.